STORAGE RELIABILITY ANALYSIS OF SOLID ROCKET PROPELLANTS

A THESIS SUBMITTED TO
THE GRADUATE SCHOOL OF NATURAL AND APPLIED SCIENCES
OF
MIDDLE EAST TECHNICAL UNIVERSITY

BY

MEHMET SİNAN HASANOĞLU

IN PARTIAL FULFILLMENT OF THE REQUIREMENTS
FOR
THE DEGREE OF MASTER OF SCIENCE
IN
MECHANICAL ENGINEERING

AUGUST 2008

Approval of the thesis:

STORAGE RELIABILITY ANALYSIS OF SOLID ROCKET PROPELLANTS

submitted by **MEHMET SİNAN HASANOĞLU** in partial fulfillment of the requirements for the degree of **Master of Science in Mechanical Engineering Department, Middle East Technical University** by,

Prof. Dr. Canan Özgen
Dean, Graduate School of **Natural and Applied Sciences** _____

Prof. Dr. Kemal İder
Head of Department, **Mechanical Engineering** _____

Assoc. Prof. Dr. Serkan Dağ
Supervisor, **Mechanical Engineering Department, METU** _____

Dr. Özge Şen
Co-supervisor, **TÜBİTAK-SAGE** _____

Examining Committee Members:

Prof. Dr. Bülent Doyum
Mechanical Engineering, METU _____

Assoc. Prof. Dr. Serkan Dağ
Mechanical Engineering, METU _____

Dr. Özge Şen
TÜBİTAK-SAGE _____

Prof. Dr. Suat Kadıoğlu
Mechanical Engineering, METU _____

Dr. Gökhan Özgen
Mechanical Engineering, METU _____

Date: _____

I hereby declare that all information in this document has been obtained and presented in accordance with academic rules and ethical conduct. I also declare that, as required by these rules and conduct, I have fully cited and referenced all material and results that are not original to this work.

Name, Last Name: Mehmet Sinan Hasanoğlu

Signature :

ABSTRACT

STORAGE RELIABILITY ANALYSIS OF SOLID ROCKET PROPELLANTS

Hasanoğlu, Mehmet Sinan
M.S., Department of Mechanical Engineering
Supervisor : Assoc. Prof. Dr. Serkan Dağ
Co-Supervisor : Dr. Özge Şen

August 2008, 110 pages

Solid propellant rocket motor is the primary propulsion technology used for short and medium range missiles. It is also commonly used as boost motor in many different applications. Its wide spread usage gives rise to diversity of environments in which it is handled and stored. Ability to predict the storage life of solid propellants plays an important role in the design and selection of correct protective environments.

In this study a methodology for the prediction of solid propellant storage life using cumulative damage concepts is introduced. Finite element mesh of the solid propellant grain is created with the developed parametric grain geometry generator. Finite element analyses are carried out to obtain the temperature and stress response of the propellant to the environmental thermal loads.

Daily thermal cycles are assumed to be sinusoidal cycles represented by their means and amplitudes. With the cumulative damage analyses, daily damage accumulated in the critical locations of the solid propellant grain are investigated. Meta-models relating the daily damage amount with the daily temperature cycles are constructed in order to compute probability of failure.

The results obtained in this study imply that it is possible to make numerical predictions for the storage life of solid propellants even in the early design phases. The methodology presented in this study provides a basis for storage life predictions.

Keywords: Solid Propellant Rocket Motors, Grain Geometry, Storage Life, Storage Reliability, Cumulative Damage

ÖZ

KATI YAKITLI ROKET MOTORLARININ DEPOLAMA GÜVENİLİRLİĞİ

Hasanoğlu, Mehmet Sinan
Yüksek Lisans, Makina Mühendisliği Bölümü
Tez Yöneticisi : Doç. Dr. Serkan Dağ
Ortak Tez Yöneticisi : Dr. Özge Şen

Eylül 2008, 110 sayfa

Katı yakıtlı roket motorları, kısa ve orta erimli roketlerde en yaygın kullanılan itki sistemleridir. Diğer birçok uygulamada da fırlatma motoru olarak kullanılırlar. Bu denli yaygın kullanımları, birçok farklı çevre koşullarında kullanılmaları ve depolanmalarını gerektirir. Katı yakıtların depolama ömrünün kestirilebilmesi, tasarım aşamasında ve uygun koruyucu ortamın belirlenmesinde önemli rol oynar.

Bu çalışmada, birikmiş hasar kavramları kullanılarak katı yakıtların depolama ömürlerinin kestirilmesi için bir yöntemler dizisi sunulmuştur. Katı yakıt çekirdeğinin sonlu elemanlar ağı, geliştirilen parametrik yakıt çekirdeği geometri üreticisi yardımıyla oluşturulmuştur. Yakıt çekirdeğinin çevresel ısıl yüklere olan ısıl ve yapısal cevabı sonlu elemanlar çözümlemeleriyle bulunmuştur.

Günlük ısıl çevrimlerin, ortalamaları ve genlikleriyle ifade edilen sinüsoidal çevrimler olduğu varsayılmıştır. Birikmiş hasar çözümlemeleriyle, yakıt çekirdeğinin kritik bölgelerinde biriken günlük hasar miktarları incelenmiş, başarısızlık olasılığının hesaplanabilmesi için günlük hasar miktarlarını, günlük ısıl çevrimlere bağlayan meta-modeller oluşturulmuştur.

Bu çalışmada elde edilen sonuçlar, erken tasarım evrelerinde bile katı yakıtların depolama ömürleriyle ilgili tahminlerin yapılabileceğine işaret etmektedir. Bu tez çalışmasında sunulan yöntemler dizisi, depolama ömrünün kestirimi için bir temel oluşturmaktadır.

Anahtar Kelimeler: Katı Yakıtlı Roket Motorları, Yakıt Çekirdeği Geometrisi, Depolama Ömrü, Depolama Güvenilirliği, Birikmiş Hasar

To my fiancée, İmran, with love...

ACKNOWLEDGMENTS

I would like to express my gratitude to all those who gave me the possibility to complete this thesis. I would like to express my deepest thanks and appreciation to my supervisor, Assoc.Prof.Dr.Serkan DAĞ, and my co-supervisor, Dr.Özge ŞEN, for their supervision and support.

This work would not have been possible without the support and encouragement of my former chief, Mr.Bayındır KURAN, under whose supervision I chose this topic and began the thesis. I have furthermore to thank the head of Propulsion and Warhead Technologies Group at TÜBİTAK-SAGE, Dr.Mehmet Ali AK, for his inspiration and support.

I offer my sincerest gratitude to my chief, Mr.Kenan BOZKAYA, who has supported me thoughout my thesis with his patience. I have been blessed with a friendly, helpful, and understanding group of colleagues. My special thanks are to Banu AYTEKİN and Mümtaz Afşin ESİ for guiding me through the challenges, and giving me a helping hand whenever I needed. Many thanks also to Taner BUDAK, for something greater: a friendly smile.

I also want to thank Prof.Dr.İhsan SOLAK for his help in mathematics.

TÜBİTAK-SAGE, who supported this work and made it possible is also greatly acknowledged.

I cannot end without thanking my family, who never denied their love and support throughout my life. Their unflinching determination and generosity will always inspire me. I also would like to thank my fiancée for always being there for me.

TABLE OF CONTENTS

LIST OF TABLES

TABLES

LIST OF FIGURES

FIGURES

LIST OF SYMBOLS

$\bar{y}$	Average of response values
β	Cumulative damage exponent
Δt_i	Time that the specimen is exposed to the i^{th} stress level
η	Viscosity
μ_d	Mean of daily damage
μ_m	Mean of mothly damage
μ_y	Mean of yearly damage
μ_{yt}	Mean of time dependent yearly damage
ν	Poisson's ratio
σ_0	Reference stress
σ_d	Standard deviation of daily damage
σ_m	Standard deviation of monthly damage
σ_y	Standard deviation of yearly damage
σ_{yt}	Standard deviation of time dependent yearly damage
σ	Stress
τ_r	Relaxation time

τ_r	Retardation time
ε	Strain
ζ	Reduced time
a_T	Shift factor
C	Elastic modulus tensor
C_1	WLF shift function coefficient 1
C_2	WLF shift function coefficient 2
D	Damage
E	Relaxation modulus, Young's modulus
F	Probability of failure
G	Shear modulus
H	Heaviside step function
J	Compliance
K	Bulk modulus
k	Boltzmann constant
LS	Limitstate function
n_{days}	Number of days in a month
R^2	Coefficient of determination
S	Sigmoid function

SS_E Sum of squared errors

SS_T Sum of squares respectively

T_0 Reference temperature

t_{fi} Mean time to failure when the specimen is subjected only to i^{th} stress level

T_{ref} Reference temperature

U Activation energy

W Stored energy density

CHAPTER 1

INTRODUCTION

This chapter gives a brief overview of solid propellant motors. General characteristics of solid propellant motors and its subcomponents are placed into this context.

The use of solid propellant rockets spans many years. Even though there is a growing interest in other propulsion technologies, solid propellant rocket still supplies propulsion for a wide range of missiles. Numerous solid propellants are in service or development and the future of solid propellants seems to be assured.

Solid propellant rocket motor is the primary propulsion technology used for short and medium range missiles. Although long range missiles generally utilize turbojet, ramjet or ramrocket technologies, these propulsion technologies carry the need for a solid propellant boost motor to accelerate the missile to a velocity sufficient to sustain air breathing propulsion mode.

Within the wide range of topics related to solid propellant rockets, grain structural integrity still remains a challenging area for design engineers. It is the key discipline that governs performance, reliability, and service life. The ability to predict the structural behavior of the grain in long term is vital when growing pressure for longer service life is considered.

1.1 General Characteristics

Vast majority of the missiles in service use solid propellant motors for propulsion. These motors, in most of the cases, represent 50 - 60% of the total mass of the missile [1]. Solid rocket motors produce very high powers. Short to medium range flight profiles attained with solid rockets are impossible with other types of propulsion technologies. However, in long

range applications solid rocket motors become unacceptably heavy and air breathing motors are preferred.

The property of solid rocket that governs the flight characteristic is thrust-time profile. Thrust-time profile of a solid rocket is predetermined and implemented by the grain geometry. Varying profiles meeting requirements of different stages of the flight can be obtained from a single solid propellant grain.

When compared with liquid propellant rockets or airbreathing propulsion systems, solid rocket motors are much simpler in design. They have very few parts and require almost no maintenance. However, they have to withstand more severe conditions than any other propulsion system due to their high power output and varying operating conditions. Since the solid rocket is a one-shot device, it is impossible to test its main element, the propellant grain, before operation. Furthermore, failure of the propellant grain generally leads to excessive combustion pressures which in turn cause the rupture of the motor case or other catastrophic failures [1]. Therefore, design for high levels of reliability is clearly needed.

1.2 Elements of a Solid Propellant Rocket Motor

A typical solid rocket motor configuration is shown in Figure 1.1. When ignited, solid propellant burns and produces hot gas that pass through a nozzle to provide thrust. Main structural elements of the solid propellants are mentioned briefly in the following sections.

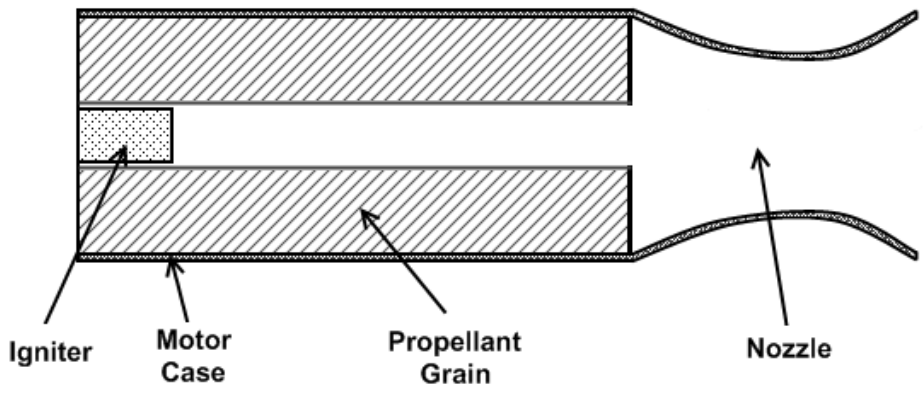

Figure 1.1: Solid Rocket Motor Configuration

1.2.1 Grain

The main objective of the grain design is to meet the thrust-time profile dictated by the missile design while guaranteeing structural integrity of the grain during storage, handling, transportation, and operation of the rocket motor. The thrust-time profile depends mainly on the burning surface area of the grain and properties of the propellant such as burn rate and density. High level of dependency of the thrust-time profile to the grain geometry in conjunction with the wide variety of thrust-time profile requirements of different types of missiles gives rise to a wide range of grain geometry configurations. However, there are further design constraints that grain geometry affects such as stress levels within the propellant, manufacturing ease, and combustion stability. Therefore there is a set of grain geometries which, by experience, is known to withstand severe environments and give the designer the ability to meet with various thrust profiles when appropriately configured. Some of these geometries are shown in Figure 1.2.

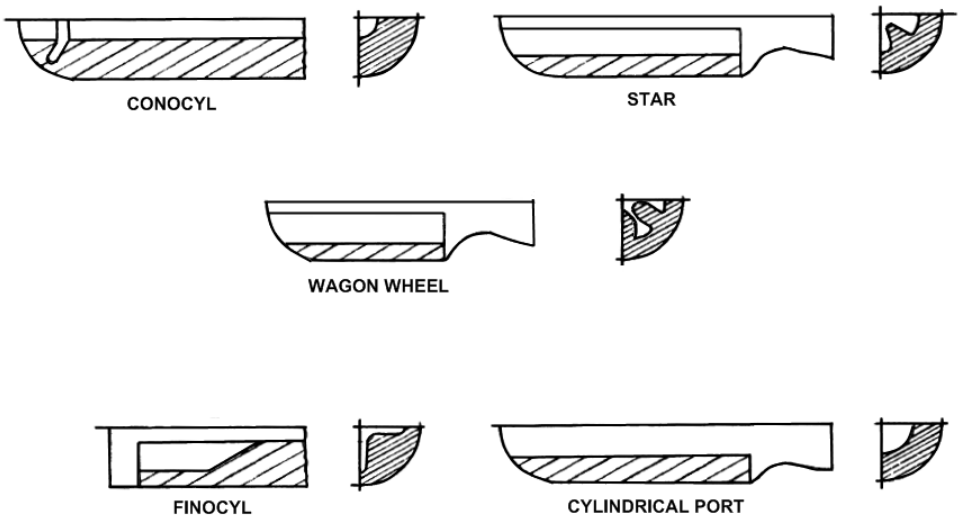

Figure 1.2: Several types of grain geometries [2]

The grain design must be evaluated for structural integrity and ballistics. Both analyses are complicated numerical tasks which require high speed computers and capable CAD software. Modern tools should enable integrated modeling / structural analysis / ballistic analysis.

Solid propellant grains may be cast directly into the internally insulated motor case or they may be cast in molds to be fixed in the motor case later by mechanical or chemical bonds.

Grain configurations explained above are called case bonded and free standing grains respectively [3]. Although free standing grains have lower volumetric efficiencies, they may be configured to have very large burning areas. Therefore, they are generally used when larger thrust for a shorter time is required [3]. As the name implies case bonded grains are directly bonded to the motor case. Internal conduit of the grain is obtained by the use of a mandrel in the casting process. When propellant is fully cured mandrel is removed to leave the finished grain. As well as having higher volumetric efficiencies, case bonded grains also help protecting the motor case from excessive heat since the propellant itself is a very good insulator. However the large difference between the thermal expansion coefficients of the grain and the case strongly influence the stress/strain state off the grain under thermal and pressure loads [1]. Special geometric features called stress relievers are implemented in several regions of the grain to overcome this problem. Almost all of the case bonded grains have central conduits and burn radially to reduce stresses.

1.2.2 Propellant

Solid rocket propellant is basically a fuel-oxidizer mixture in solid state. It's not only the energy source of the propulsion system but also is a structural element of it. Therefore, some idealized requirements when developing or selecting a propellant for a given application may be listed as follows [1]:

- The propellant should have sufficient burning rate at the design pressure with a low pressure and temperature dependency.
- It should have a high specific impulse[1] and density.
- It should easily be ignited by the use of an igniter while being insensitive to other disturbances for safety reasons.
- The propellant must provide ease of manufacturing and be suitable for being formed into different grain geometries and configurations.
- Its mechanical properties should be acceptable over a wide temperature range.

[1] Specific impulse represents the change in momentum per unit weight of propellant. It is a measure of the efficiency of rocket motors.

- Its properties should not deteriorate with age or environmental effects.

Meeting all of the requirements listed above is very difficult. After years of experience two main categories of propellants which provide sufficient characteristics have emerged. These are double-base and composite propellants.

1.2.2.1 Double-Base Propellant

Double base propellant consists of two base propellants namely nitro-cellulose and nitroglycerine. Oxidizer and fuel are the parts of a single molecular chain in the case of double base propellant. Therefore a chemical bond exists between the oxidizer and the fuel. Double base propellants have a tendency to unstable burning requiring addition of stabilizers like particulate matter or use of mechanical baffles and damping devices in the chamber. Plasticizing agents and small quantities of metal salts are also added at production stages for enhancing mechanical properties and providing some burning rate control.

Double base propellants are generally prepared in large mixers with large amounts of solvents. Afterwards, they are shaped by extruding through dies. After the extrusion process, the propellant is dried to remove excess solvent [3]. Double base propellants are generally free standing in the motor case.

Double base propellants are used for smaller rocket motors with simple grain geometries where high trust for short period of time is required. Obtaining complex geometries through extrusion of the double base propellant is nearly impossible. Therefore, its use is very rare in larger rocket motors or applications where more controlled burning is desired.

1.2.2.2 Composite Propellants

Most commonly used propellant in rocket motors is the composite propellant. The term composite implies that the propellant is the heterogeneous mixture of its components with no chemical bond connecting them. Composite propellants are based on a binder which also serves as fuel and encompasses solid oxidizer. Almost all of the modern composite propellants for missiles use hydroxyl-terminated polybutadiene (HTPB) as a binder since HTPB offers the optimum combination of thermodynamic and mechanical properties [1]. However,

there are other materials used as a binder such as carboxy-terminated polybutadiene (CTPB) or polyurethane. These binder materials had been used in earlier rocket motors and their usage was limited due to their inferior mechanical properties compared to HTPB. In large space systems a polybutadiene - acrylic acid acrylonitrile (PBAN) is commonly used. Ammonium perchlorate (AP) is used as the oxidizer in composite propellants with almost no exception [1]. It can be easily obtained and it enables milling to a range of particle sizes thus providing control over burning rate.

Composite propellants are produced by casting directly into the motor case or a die. After the ingredients are mixed and cast into the case, the propellant is baked for up to a week until it solidifies. This process is commonly called curing. After curing is completed, mandrel, if used for inner conduit shaping, is removed to leave the propellant at the desired geometry. Therefore, complex grain shapes can be obtained through casting of composite propellants.

1.2.3 Motor Case

The motor case is the structural framework of the solid rocket motor. It supports the bonded or free standing grain together with all of the components forming the rocket motor. Most common type of motor case is monolithic metallic case. This type of case employs high strength metals such as steel, aluminum, and titanium.

Since the propellant burns within the motor case, it is subjected to very high pressures such as 100 bars or more [3]. Motor case may also be subjected to extreme levels of high temperature and inertial forces. These severe conditions require high strength materials and design for high levels of reliability.

1.2.4 Igniter

As mentioned before solid propellants are made insensitive for safety reasons. Therefore, a more sensitive igniter is required to ignite the propellant. Igniters usually consist of a primary charge ignited by a resistive electric wire and a secondary more energetic charge to ignite the propellant.

The ignition process starts with passage of an electrical current through the wire located in

the primary charge so called “squib”. When the electric wire heats, the touching sensitive energetic material ignites and starts the ignition process. The process continues with the secondary charge and finally the propellant.

The whole ignition process takes some time. Ignition process contains combustion, flow, heat transfer processes as chain events. All these processes require certain amount of time to realize. Therefore, there is a time lag between the ignition signal and the actual ignition called the “ignition delay”.

1.3 Service and Storage Environments

Solid rockets are commonly used with land, air, and sea platforms. Their wide spread usage gives rise to diversity of environments they are handled and stored.

For land and air based systems the thermal environment prior to operation is governed by the climate of the storage or deployment location. Solid propellants in this case may be stored in very different configurations ranging from unsheltered storage to temperature controlled magazines [1]. Some of the sea based systems may favor controlled storage environments where others are exposed to harsh marine environments.

The climatic temperature models are generally cyclic in nature. They suggest diurnal temperature cycles and their probabilities of occurrence. However, in unsheltered, unshaded conditions or storage in containers, solar radiation and temperature rises should be accounted for [18].

Furthermore, in air-carried systems special types of environmental disturbances such as captive carriage vibrations and aerodynamic heating should be taken into account.

1.4 Scope of the Study

In this study, development of a methodology for prediction of service life of solid propellants is aimed. For this purpose, thermal stresses that are induced by the environmental thermal loads are investigated. Affects of gravitational loads are also evaluated and found to be unimportant when compared with thermal stresses.

To be able to investigate service life of different grain configurations, a parametric grain geometry generator is developed and is coupled with an external meshing tool to obtain finite element meshes for structural analysis. The temperature field of the propellant during storage is also calculated with a simplified 2D finite element analysis. The temperature field is then used in structural analysis to obtain the structural response of the propellant grain.

Daily temperature changes are assumed to be cyclic and a methodology for predicting the amount of damage that is accumulated during a daily temperature cycle is developed. Meta-models, emulating this thermo-structural relation are constructed for further statistical investigations. Response Surface and Artificial Neural Network methodologies are used for the construction of these meta-models which are used for estimation of the probability of failure of the propellant grain.

In addition to studies found in literature, the propellant storage life prediction techniques are combined with parametric grain geometry generation. Furthermore, meta-models are constructed for further statistical investigations such as statistical characterization of the damage with Monte Carlo simulations.

CHAPTER 2

LITERATURE SURVEY

This chapter puts together the theoretical background enabling analysis of the stored solid propellant. Theoretical reference on the unique material behavior of solid propellants is given in detail. A comprehensive investigation of the past studies is also presented.

2.1 Viscoelastic Solids

Solid propellants are categorized as viscoelastic solids. Viscoelastic materials are unique in behavior exhibiting both viscous and elastic characteristics. Viscous materials resist strain linearly with time when a stress is applied. Therefore, their behaviors are time dependent, whereas, elastic materials respond instantaneously to the applied stress. Viscoelastic material behavior is a mixture of the two. Whereas elasticity is usually the result of bond stretching along crystallographic planes in an ordered solid, viscoelasticity is the result of the diffusion of atoms or molecules inside of an amorphous material [4].

2.1.1 Viscoelastic Phenomena

For small strains most of the engineering materials are described by Hooke's law of linear elasticity. Hooke's law states that the stress σ is proportional to strain ϵ. In one dimension, Hookes law is as follows:

$$\sigma = E\varepsilon \tag{2.1}$$

E in the above equation is the Young's modulus. Equation 2.1 can also be written in terms of the compliance J:

$$\varepsilon = J\sigma \tag{2.2}$$

These relations are valid for elastic materials. Viscous fluids behave differently. A viscous fluid under shear stress obeys the following relation:

$$\sigma = \eta \frac{d\varepsilon}{dt} \tag{2.3}$$

Viscoelastic materials deviate from Hooke's law by exhibiting viscous-like as well as elastic characteristics. For viscoelastic materials, the relationship between stress and strain depends on time.

Some phenomena in viscoelastic materials must be stated for better understanding of viscoelasticity [6]:

1. If the stress is held constant, the strain increases with time. (Creep)
2. If the strain is held constant, stress decreases with time. (Relaxation)
3. The effective elasticity modulus depends on the rate of application of the load.
4. In case of cyclic loading, a phase lag occurs between the loading and dynamic response. This phenomena causes dissipation of energy.
5. Acoustic waves traveling in viscoelastic material experience attenuation.
6. Rebound of an object after impact is less than 100%.
7. During rolling of a viscoelastic material, frictional resistance is observed.

2.1.2 Creep

Creep is time dependent, progressive deformation of a material under constant stress. Since the phenomenon is time dependent the loading history must be known to describe creep be-

havior of a material. Suppose the history of stress σ is defined to be a step function starting at $t = 0$:

$$\sigma(t) = \sigma_0 \mathrm{H}(t) \tag{2.4}$$

The strain $\sigma(t)$ in a viscoelastic material will increase in time with the ratio called creep compliance.

$$J(t) = \frac{\varepsilon(t)}{\sigma_0} \tag{2.5}$$

As can be seen in equation 2.5 the creep compliance depends on the stress level σ_0. However, this is the case for non-linear viscoelastic materials. For linear viscoelastic materials creep compliance is independent of the stress level. If the load is removed at a later time the strain will recover, or deformation will progressively decrease. Strain at recovery may or may not reach zero depending on the material.

Elastic materials constitute a special case in which the creep compliance is also a step function of the form:

$$J(t) = J_0 \mathrm{H}(t) \tag{2.6}$$

Elastic materials immediately recover to zero strain when the load is released. There also are some viscoelastic materials that recover to zero strain after sufficient time. These materials are called anelastic.

Viscous materials constitute another special case for which the creep compliance can be defined as follows:

$$J(t) = \eta t \mathrm{H}(t) \tag{2.7}$$

As mentioned before, viscoelastic material behavior is a mixture of viscous and elastic behavior. This can easily be seen in Figure 2.1 where creep response of elastic, viscous, and viscoelastic materials are compared.

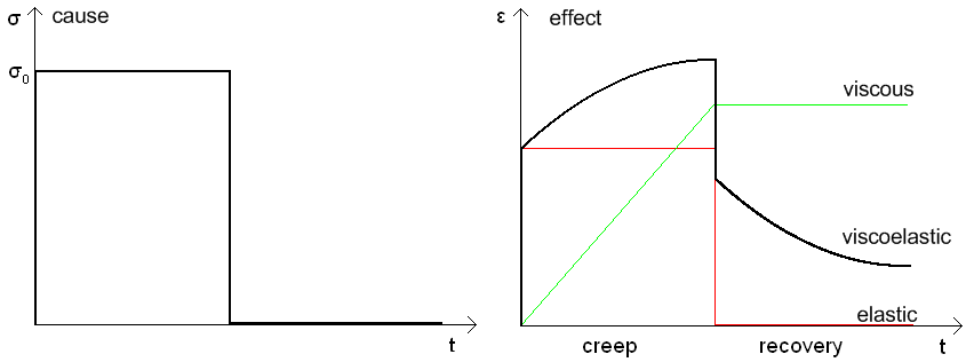

Figure 2.1: Creep responses of different materials

Creep can be considered to have three regions. In the primary creep region the creep curve is concave down. In secondary creep, deformation is proportional to time. Finally, in the tertiary creep the deformation increases with time until creep rupture occurs (Figure 2.2).

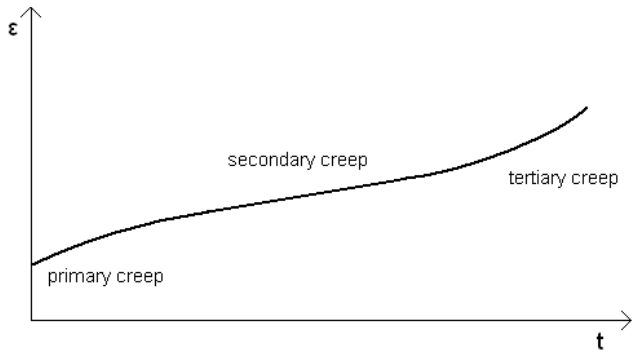

Figure 2.2: Creep stages

2.1.3 Stress Relaxation

As mentioned before stress relaxation is the gradual decrease in the stress when the material is kept at constant strain. With a similar approach applied for creep, we can define the strain history to be a step function starting from $t = 0$:

$$\varepsilon(t) = \varepsilon_0 \mathrm{H}(t) \tag{2.8}$$

The stress in the material will decrease with a ratio called the relaxation modulus $E(t)$.

$$E(t) = \frac{\sigma(t)}{\varepsilon_0} \tag{2.9}$$

In this case it can be seen from the equation 2.9 that the relaxation modulus depends on the strain level. However, this dependency is valid for only non-linear viscoelastic materials. For linear material $E(t)$ is only a function of time.

Stress relaxation behaviors of viscoelastic and elastic materials can be seen in Figure 2.3.

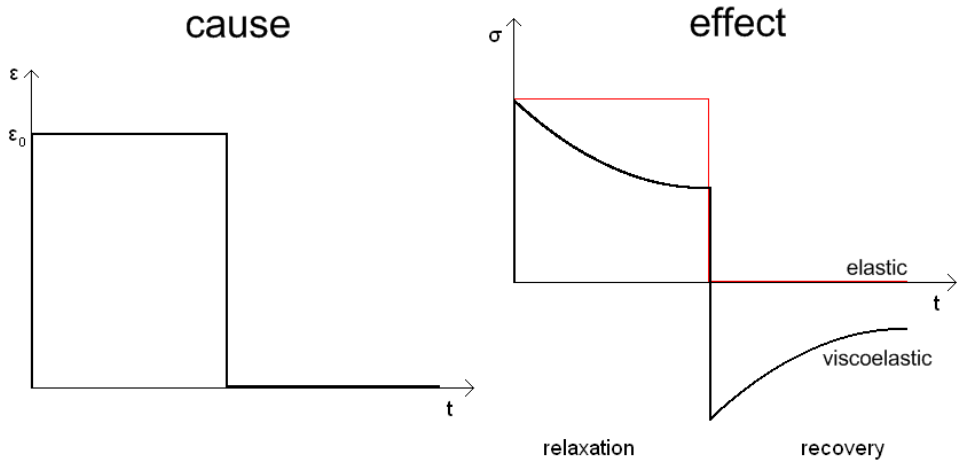

Figure 2.3: Stress relaxation of different materials

2.1.4 Constitutive Behavior

In the previous sections response of the material to the cases of step stress or step strain was defined. Constitutive equations are developed to predict the response of the material to any stress or strain history.

2.1.4.1 Response of linear viscoelastic material

Constitutive equation for linear viscoelastic materials are developed using the Boltzmann superposition principle. Boltzmann states that the effect of a complex cause is the sum of effects of the individual causes constituting the complex cause. First consider the stress response for a known strain history. Recall the equations 2.8 and 2.9.

$$\varepsilon(t) = \varepsilon_0 \mathrm{H}(t)$$
$$E(t) = \frac{\sigma(t)}{\varepsilon_0}$$

Assume a strain history having the shape of a boxcar function from $t1$ to $t2$. The assumed strain can be written as a superposition of two step functions (Figure 2.4).

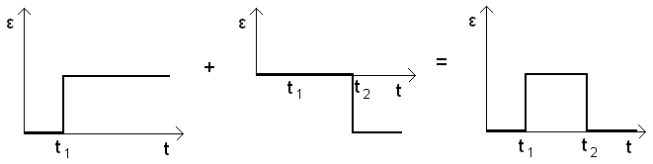

Figure 2.4: Boxcar function

The strain history seen in Figure 2.4 can be formulated as:

$$\varepsilon(t) = \varepsilon_0 \left[\mathrm{H}(t - t_1) - \mathrm{H}(t - t_2)\right] \tag{2.10}$$

Stress can be written using Boltzmann superposition principle and equation 2.9.

$$\sigma(t) = \varepsilon_0 \left[E(t - t_1) - E(t - t_2)\right] \tag{2.11}$$

These relations are only valid for nonaging materials. Material properties of the aging materials change in time.

Consider a segment of strain history from time τ to time $\tau + \Delta\tau$. The value of strain within this strain increment is defined as ε_0 (Figure 2.5). Since it's a segment of history the strain in this increment affects the stress to the time considered as "now" which is denoted by t.

$$\varepsilon(t) = \varepsilon_0 \left[\mathrm{H}(t - \tau) - \mathrm{H}(t - \tau - \Delta\tau)\right] \tag{2.12}$$

The stress resulting from the increment of strain history can be formulated as it had been in equation 2.11.

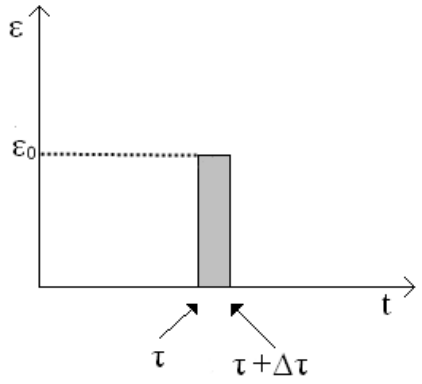

Figure 2.5: Strain increment

$$\sigma(t) = \varepsilon_0 \left[E(t-\tau) - E(t-\tau-\Delta\tau)\right] \tag{2.13}$$

If we consider a strain history being composed of small strain increments of the same size ($\Delta\tau$), Boltzmann superposition principle lets us to formulate the stress at time t (now) resulting from the whole strain history as follows (Figure 2.6).

$$\sigma(t) = \sum_i \varepsilon_i \left[E(t-\tau_i) - E(t-\tau_i-\Delta\tau)\right] \tag{2.14}$$

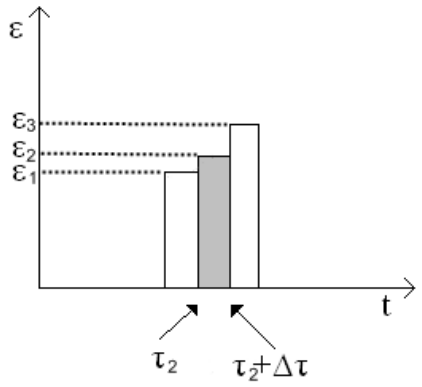

Figure 2.6: Strain history represented in increments

Equation 2.14 gives the stress response at time t to a strain history consisting of increments of boxcar functions. If we assume that the boxcar functions are approximations of an actual

continuous differentiable strain history $\varepsilon(t)$ (Figure 2.7), we can relate the strain levels of each strain increment to the time variable as follows.

$$\varepsilon_i = \varepsilon\left(\tau_i + \frac{\Delta\tau}{2}\right) \tag{2.15}$$

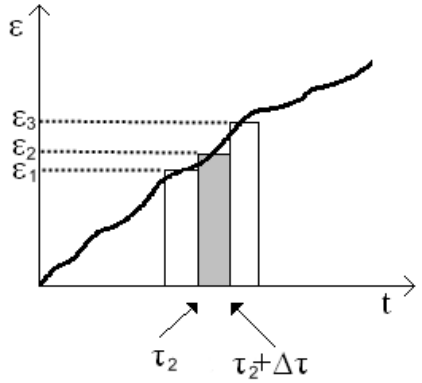

Figure 2.7: Strain history represented in increments

Therefore, we can now write equation 2.14 in the following form.

$$\sigma(t) = \sum_i \varepsilon\left(\tau_i + \frac{\Delta\tau}{2}\right)[E(t-\tau_i) - E(t-\tau_i-\Delta\tau)] \tag{2.16}$$

Consider the following derivative.

$$\frac{dE(x)}{d\tau} = \frac{dE(x)}{dx}\frac{dx}{d\tau} \quad where \quad x = t - \tau \tag{2.17}$$

Note that since we are seeking the stress response at time t for the strain history, t is not an independent variable in the expression above. Therefore, since

$$\frac{dE(x)}{dx} = \lim_{\Delta x \to 0} \frac{E(x+\Delta x) - E(x)}{\Delta x}$$
$$\Delta x = \Delta t - \Delta\tau = -\Delta\tau$$
$$\frac{dE(x)}{dx} = \lim_{\Delta\tau \to 0} \frac{E(t-\tau-\Delta\tau) - E(t-\tau)}{-\Delta\tau}$$
$$\frac{dx}{d\tau} = -1$$

the derivative in equation 2.17 becomes

$$\begin{aligned} \frac{dE(x)}{d\tau} &= -1.\lim_{\Delta\tau\to 0}\frac{E(t-\tau-\Delta\tau)-E(t-\tau)}{-\Delta\tau} \\ \frac{dE(t-\tau)}{d\tau} &= \lim_{\Delta\tau\to 0}\frac{E(t-\tau-\Delta\tau)-E(t-\tau)}{\Delta\tau} \end{aligned} \tag{2.18}$$

So to obtain the stress response for a continuous strain history, as $\Delta\tau$ approaches to zero, according to equation 2.18, equation 2.16 becomes:

$$\sigma(t) = -\int_0^t \varepsilon(\tau)\frac{dE(t-\tau)}{d\tau}d\tau \tag{2.19}$$

Equation 2.19 describes the effect of the whole strain history on the stress. Effect of the strain at time t has to be included too. Therefore,

$$\sigma(t) = -\int_0^t \varepsilon(\tau)\frac{dE(t-\tau)}{d\tau}d\tau + E(0)\varepsilon(t) \tag{2.20}$$

The above equation describes the stress at time t resulting from the strain history from time 0 to t and the strain at time t itself. However the term $\dot{E}(t-\tau)$ makes it very difficult to use in numerical calculations. In order to obtain a more useful form of this equation we shall integrate the equation 2.20 by parts, assuming $\varepsilon(0) = 0$ to obtain a more useful equation:

$$\sigma(t) = \int_0^t E(t-\tau)\frac{d\varepsilon(\tau)}{d\tau}d\tau \tag{2.21}$$

The expression above, so called the ”hereditary integral” of the constitutive response, is the most suitable expression for relating stress with strain history since it doesn't contain the derivative of the relaxation modulus and the strain derivation is performed at τ instead of $t-\tau$. However, the hereditary integral is only valid when $\epsilon(0) = 0$. Also note that there is no strain history before $t = 0$. As will be explained in the following sections, relaxation modulus of a viscoelastic material is not only a function of time but also a function of temperature history. Therefore, the relaxation modulus should be in its simplest form for numerical evaluations.

Another form of the "hereditary integral" can also be derived for strain response of a known stress history just by changing the roles of stress and strain.

$$\varepsilon(t) = \int_0^t J(t-\tau)\frac{d\sigma(\tau)}{d\tau}d\tau \tag{2.22}$$

Note that in the hereditary integral the history of the cause starts at time zero. Before that the cause does not exist.

2.1.5 Physical Restrictions on the viscoelastic functions

The stored energy density of linearly viscoelastic materials have the form [5]:

$$W(t) = \frac{1}{2}\int_{-\infty}^{t}\int_{-\infty}^{t}\frac{\partial}{\partial t}E(2t-\tau-\eta)\frac{d\varepsilon}{d\tau}\frac{d\varepsilon}{d\eta}d\tau d\eta \tag{2.23}$$

Since the thermodynamic principle states that the dissipation rate of energy is nonnegative the following inequality must be satisfied.

$$-W(t) \geq 0 \tag{2.24}$$

For the energy dissipation to be nonnegative during relaxation the following conditions must exist.

$$E(t) \geq 0 \tag{2.25}$$

$$\frac{dE(t)}{dt} \leq 0 \tag{2.26}$$

In a material which exhibits fading memory the magnitude of the effect of a more recent cause is greater than the magnitude of the effect of a cause of identical magnitude in the distant past [6]. Therefore,

$$\left|\frac{dE(t)}{d(t)}\right|_{t=t_1} \leq \left|\frac{dE(t)}{d(t)}\right|_{t=t_2} \quad for\ t_1 > t_2 > 0 \tag{2.27}$$

Equation 2.27 requires the derivative to decrease in time. Consequently, if the derivative decreases with time the material exhibits fading memory.

$$\frac{d^2E(t)}{dt^2} \geq 0 \tag{2.28}$$

A relation between relaxation function $E(t)$ and creep function $J(t)$ can be found through Laplace transform of the equations 2.21 and 2.22 [6].

$$\frac{\sigma(s)}{\varepsilon(s)} = sE(s) \quad and \quad \frac{\sigma(s)}{\varepsilon(s)} = \frac{1}{sJ(s)} \tag{2.29}$$

Therefore the following relation in laplace domain is found. The relation between relaxation and creep functions in time domain is found by inverse transformation of the relation in laplace domain by convolution theorem.

$$\begin{gathered} E(s)J(s) = \frac{1}{s^2} \\ \int_0^t J(t-\tau)E(\tau)d\tau = \int_0^t E(t-\tau)J(\tau)d\tau \end{gathered} \tag{2.30}$$

2.1.6 Mechanical Models

There are mainly four different mechanical models describing viscoelastic material behavior. Since their behavior exhibit both viscous and elastic characteristics, viscoelastic mechanical models are composed of ideal springs and dampers in various configurations.

2.1.6.1 Maxwell model

The Maxwell model consists of a spring and a damper in series as shown in Figure 2.8. It is named after Scottish mathematician and theoretical physicist, James Clerk Maxwell after he proposed Maxwell model also known as the Maxwell material in 1867.

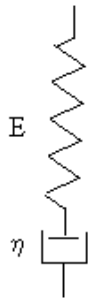

Figure 2.8: Maxwell element

The relaxation response in case of a step strain in Maxwell model is [6]

$$E(t) = Ee^{-t/\tau_r} \tag{2.31}$$

Here, τ_r is called the relaxation time defined as $\tau_r = \eta/E$

Although, the relaxation response seen in equation 2.31 is close to the actual material behavior, the creep response in case of step stress for this model is as follows.

$$J(t) = \frac{1}{E} + \frac{t}{\eta} \tag{2.32}$$

Creep function of the Maxwell model as seen in 2.32 is not realistic since it is a linear function of time. Experimental results on creep behavior of viscoelastic materials show curvatures. Relaxation and creep behaviors of the Maxwell material can be seen in Figure 2.9.

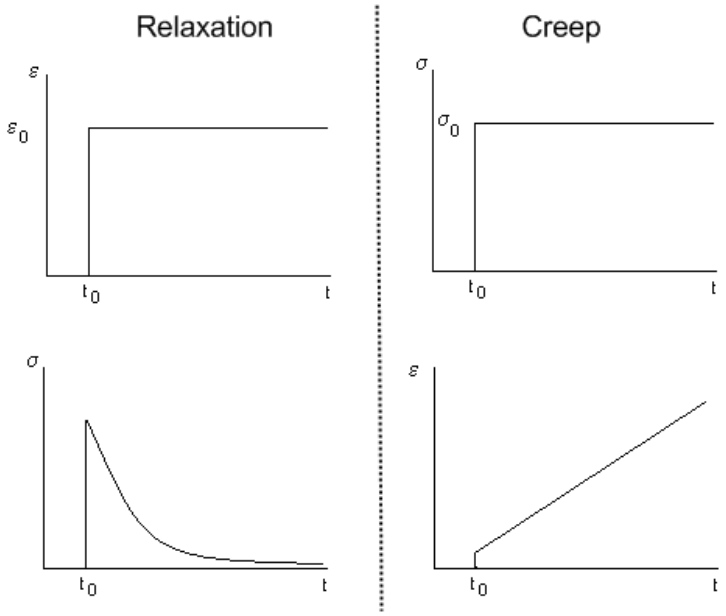

Figure 2.9: Maxwell element creep and relaxation functions

2.1.6.2 Voigt Model

Voigt model, also known as the Kelvin model, consists of a spring and a damper in parallel as seen in Figure 2.10. It is named after the German physicist Woldemor Voigt and British physicist Kelvin, Lord William Thomson.

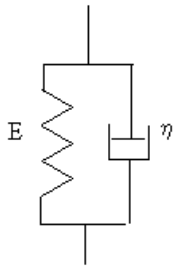

Figure 2.10: Voigt material model

The creep function for the Voigt model is

$$J(t) = \frac{1}{E}\left(1 - e^{-t/\tau_c}\right) \tag{2.33}$$

Where, τ_c is called the retardation time defined as $\tau_c = \eta/E$.

Even though the creep function seems to be consistent with reality, the relaxation function cannot be explained since it is predicted as a constant delta function [6].

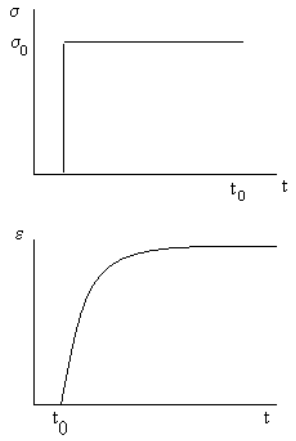

Figure 2.11: Voigt model creep function

2.1.6.3 Standart Linear Model

The standard linear model combines a Maxwell element with an ideal spring in parallel (Figure 2.12). As mentioned before Maxwell model fails to predict the creep behavior and Voigt model fails in stress relaxation. Standard linear model, being more complex than its predecessors, is the simplest material model which can represent both relaxation and creep.

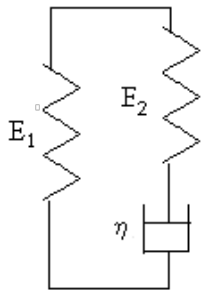

Figure 2.12: Standard linear element

The relaxation and creep functions of the standard linear model are given as follows [6]:

$$E(t) = E_1 + E_2 e^{-t/\tau_r} \tag{2.34}$$

$$J(t) = \frac{1}{E_1} + \frac{E_2}{E_1(E_1 + E_2)} e^{-t/\tau_c} \tag{2.35}$$

Where $\tau_r = \frac{\eta}{E_2}$ and $\tau_c = \tau_r \frac{E_1+E_2}{E_1}$

The relaxation and creep functions defined for standard linear material model are able to represent the actual material to some extent. However, relaxation functions with a single exponential term fail to approximate actual relaxation behavior.

2.1.6.4 Generalized Maxwell

The generalized Maxwell model also known as the Maxwell-Weichert model consists of a spring and N number of Maxwell element in series. It is named after Maxwell and German engineer Dieter Weichert. The schematic representation of a generalized Maxwell model can be seen in Figure 2.13.

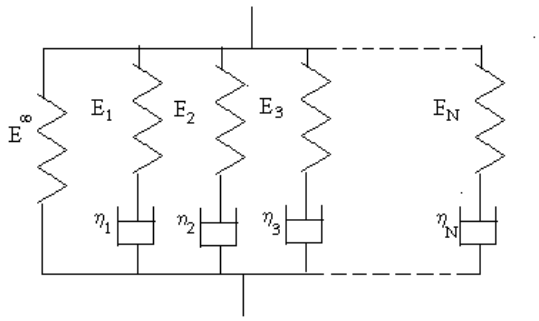

Figure 2.13: Generalized maxwell model

Generalized Maxwell is the most general form of the models described above. In contrast with the standard linear model it takes into account that the relaxation occurs over a distribution of time instead of a single time by introducing unlimited number of exponential terms to the relaxation function.

The relaxation function for the generalized Maxwell model is the sum of the relaxation functions of its elements.

$$E(t) = E^{\infty} + \sum_{i=1}^{N} E_i e^{-t/\tau_i} \tag{2.36}$$

This series representation of the relaxation function is called the Prony series.

Creep response of the generalized Maxwell model is more complicated compared with previous models. However, it can be evaluated numerically.

2.1.7 Effect of temperature

The constitutive behavior explained so far was under the assumption of isothermal conditions. Generally, viscoelastic functions of materials vary with temperature. For example the relaxation function, in fact is a function of time and temperature $E = E(t, T)$. Viscoelasticity arises from the phenomena of molecules reorganizing themselves under stress. This kind of processes depends on the speed of molecular motion which is quantified as temperature [6]. When all the processes contributing to viscoelasticity are assumed to be effected to same extend by the temperature, we have a relaxation function of the following form [6]:

$$E(t, T) = E(\zeta, T_0) \tag{2.37}$$

ζ is the reduced time.

$$\zeta = \frac{t}{a_T(T)} \tag{2.38}$$

T_0 is called the reference temperature and $a_T(T)$ is the shift factor.

Tobolsky [7] and Leaderman [8] in 1943, and Later Ferry [9] in 1950, noted that the effects of temperature and time on most homogeneous viscoelastic materials are related in a simple and convenient way. This relationship states that for a given loading, increasing the temperature produces a material response same as increasing the time. Specifically, temperature effects are experienced primarily through a temperature dependent factor multiplying the time scale [10].

For these materials including most of the viscoelastic materials, when a material property is plotted versus time, change of temperature changes just the effective time scale of the plot. For viscoelastic materials properties are usually plotted vs. log time. In such a case, change in temperature causes a horizontal shift of the material properties on the log time axis. The logarithm of the shift factor $a_T(T)$ defines the amount of shift for each temperature. Materials obeying this time-temperature superposition rule are called thermorheologically simple.

Time dependent properties of thermorheologically simple materials are therefore, characterized for a reference temperature denoted as T_0 in equation 2.37. These material properties can then be evaluated for any temperature by simply multiplying their time scale with the shift factor as seen in the equation 2.38. Shift factor is a function of temperature and equation 2.38 holds true for only fixed temperatures. If the temperature also changes with time, then the reduced time is formulated as follows [1].

$$\zeta = \int_0^t \frac{1}{a_T(T(t))} dt \tag{2.39}$$

As mentioned before the shift factor $a_T(T)$ depends on the temperature and the material. Different materials can have different temperature dependent creep behavior. Some materials obey the Arhenious relation which yields the following shift factor equation:

$$\ln\, a_T = \frac{U}{k}\left(\frac{1}{T_2} - \frac{1}{T_1}\right) \tag{2.40}$$

where U is the activation energy and k the Boltzmann constant. A more appropriate shift factor formulation for polymers which also is found to fit well to the solid propellant behavior is the empirical WLF equation (Williams, Landel, Ferry).

$$\log\, a_T = \frac{C_1\left(T - T_{ref}\right)}{C_2 + \left(T - T_{ref}\right)} \tag{2.41}$$

The term T_{ref} in WLF equation is the reference temperature where the shift factor is one. Coefficients C_1 and C_2 depend on the polymer type. These coefficients are generally found by regression of the data obtained from many relaxation tests performed at different temperatures. By describing the effect of the temperature by a shift factor the relaxation curve of the material

is drawn only for the reference temperature T_{ref} and curves for other temperatures can be extracted from this master curve.

This temperature dependency of the relaxation function should be introduced into the hereditary integral of the viscoelastic material. When the relaxation term $E(t-\tau)$ in equation 2.21 is observed, it is obvious that the relaxation function stands for the relaxation of the stress from $t = t - \tau$ to $t = t$. In isothermal conditions defining the relaxation function with a single argument of time was sufficient since the relaxation modulus function would only depend on the time interval between cause and effect. In non-isothermal conditions however relaxation modulus will also depend on the temperature profile between the time of cause and effect. Therefore the hereditary integral seen in equation 2.21 should be redefined as follows:

$$\sigma(t) = \int_0^t E(\tau, t) \frac{d\varepsilon(\tau)}{d\tau} d\tau \tag{2.42}$$

where the relaxation function $E(\tau, t)$ can be defined as

$$E(\tau, t) = E_{ref}\left(\frac{t-\tau}{\zeta_t(\tau, t)}\right) \tag{2.43}$$

In the expression above E_{ref} is the relaxation function at the reference temperature and $\zeta_t(\tau, t)$ is the reduced time defined as

$$\zeta_t(\tau, t) = \int_\tau^t \frac{1}{a_t(T(t))} dt \tag{2.44}$$

2.1.8 Linear Constitutive Relation in Three Dimensions

Hooke's law of linear elasticity can be expressed in the following form:

$$\sigma_{ij} = \sum_{kl} C_{ijkl}\varepsilon_{kl} \tag{2.45}$$

C_{ijkl} is the corresponding component of the elastic modulus tensor. Same analogy exists for linearly viscoelastic materials [6].

$$\sigma_{ij}(t) = \int_0^t \sum_{kl} C_{ijkl}(t-\tau)\frac{d\varepsilon_{kl}}{d\tau}d\tau \tag{2.46}$$

Notice that in this case each component of the modulus tensor can have different time dependence. Both (2.35) and (2.36) are general equations that can accommodate any extent of anisotropy. However, many materials are approximately isotropic. For isotropic elastic materials the constitutive equation becomes [6]

$$\sigma_{ij} = \lambda\varepsilon_{kk}\delta_{ij} + 2\mu\varepsilon_{ij} \tag{2.47}$$

where λ and μ are two tensorial constants called the Lamé[1] elastic constants. δ_{ij} is the Kronecker delta[2]. Lamé elastic constants can be used to define material properties like Young's modulus E, shear modulus G, bulk modulus K, and Poisson's ratio υ [11].

$$G = \mu \tag{2.48a}$$
$$E = \frac{G(3\lambda + 2G)}{\lambda + G} \tag{2.48b}$$
$$\nu = \frac{\lambda}{2(\lambda + G)} \tag{2.48c}$$
$$K = 2G\frac{1+\upsilon}{3(1-2\upsilon)} \tag{2.48d}$$

When the relations in expressions 2.48 are used to define λ and μ in equation 2.47 the following form of the constitutive relation is derived for isotropic linear elastic material [11].

$$\sigma_{ij} = 3K\left(\frac{1}{3}\varepsilon_{kk}\delta_{ij}\right) + 2G\left(\varepsilon_{ij} - \frac{1}{3}\varepsilon_{kk}\delta_{ij}\right) \tag{2.49}$$

A similar derivation can be done for the linearly viscoelastic materials to yield [6]:

$$\sigma_{ij}(t) = \int_0^t \lambda(t-\tau)\delta_{ij}\frac{d\varepsilon_{kk}}{d\tau}d\tau \; + \; \int_0^t 2\mu(t-\tau)\delta_{ij}\frac{d\varepsilon_{ij}}{d\tau}d\tau \tag{2.50}$$

[1] French mathematician Gabriel Lamé

[2] Kronecker delta: $\delta_{ij} = \begin{cases} 1 & if \quad i = j, \\ 0 & if \quad i \neq j \end{cases}$

In this case we have to consider time dependent engineering functions such as $E(t)$, $G(t)$, $\upsilon(t)$, and $K(t)$.

2.1.9 Aging

Aging can be defined as the time dependent variation of the material properties. This can be achieved through introduction of an age term into the material property functions such as the stress relaxation function. Assume that the relaxation function also depends on the age, then we would express it in the form $E(t_{age}, t-\tau)$ instead of $E(t-\tau)$.

If properly characterized, aging behaviors of viscoelastic materials are easy to apply in constitutive relations. However, characterizing aging behaviors of viscoelastic materials require detailed and timely experiments.

2.1.10 Non-Linear Viscoelasticity

For a material to be linear it has to obey linear integral equations or linear differential equations. For a material to be linearly viscoelastic, it is necessary but not sufficient for the creep or relaxation functions of the material to be independent of stress or strain.

Again, consider first an example of nonlinear elasticity where the modulus is strain dependent:

$$\sigma = f(\varepsilon)\varepsilon \tag{2.51}$$

There are several constitutive equations available for describing nonlinear viscoelastic behavior. Following is a simple nonlinear relation where relaxation function depends on strain level [6].

$$\sigma(t) = \int_0^t E(t-\tau, \varepsilon(\tau))\frac{d\varepsilon}{d\tau}d\tau \tag{2.52}$$

A similar equation where the compliance depends on the stress level can be written [6].

$$\varepsilon(t) = \int_0^t J(t-\tau, \sigma(\tau)) \frac{d\sigma}{d\tau} d\tau \tag{2.53}$$

A more complex form of nonlinearity can be introduced by taking other sources of nonlinearities into account.

$$\varepsilon(t) = \int_0^t J(t-\tau) \frac{dF}{d\tau} d\tau \tag{2.54}$$

Note that $\sigma(t)$ is replaced with a function F in the above constitutive relation. Including some common sources of nonlinearities in viscoelastic materials such as strain rate ($\dot{\varepsilon}$) and damage ($D(t)$) would give a more accurate constitutive relation [12].

$$F = F(\sigma, t, \dot{\varepsilon}, D(t)) \tag{2.55}$$

We can use Laplace transforms and the convolution theorem to derive another form of the constitutive relation given in equation 2.54 [13]:

$$F(\sigma, t, \dot{\varepsilon}, D(t)) = \int_0^t E(t-\tau) \frac{d\varepsilon(\tau)}{d\tau} d\tau \tag{2.56}$$

2.2 Viscoelastic Material Characterisation

Viscoelastic materials are materials that behave both like Newtonian fluids and solids that obey Hooke's law. Therefore, these materials have energy dissipating properties besides their elastic properties. Mechanical properties of viscoelastic materials vary with time, strain rate, and temperature.

Solid propellants consist of hard particles embedded in soft matrix material. The viscoelastic behavior in solid propellants arise not only from the polymeric matrix but also from the filler material interacting with the matrix. Solid propellants have very complex material properties such as properties that depend on temperature, time, high displacements and strains, stress

softening due to periodic loading, and transition from incompressible behavior to compressible behavior.

Reference [1] lists the material characterization tests for solid propellants as follows:

- Uniaxial compressive test
- Uniaxial tensile test
- Stress relaxation test in tension
- Thermo mechanical test for determining the coefficient of linear thermal expansion
- Dynamic mechanical analysis test to measure the glass transition temperature
- Shifting procedure for the determination of master relaxation curves.

According to Reference [1] again the following material properties must be determined for the structural analysis.

- Stress-strain relationship
- Poisson's ratio or bulk modulus
- Density
- Coefficient of linear thermal expansion
- Thermal conductivity

2.2.1 Uniaxial Stress Relaxation Tests

To determine the master curve and the shift factors of the material, many tests have to be performed at different combinations of strain rate and temperature. With the Prony series fitted to master curve used and WLF shift function fitted to shift factors, effective elasticity modulus at any temperature and any time can be found.

In the uniaxial stress relaxation tests of solid propellants, generally JANNAF specimens are used. The specimens are clamped to a tensile test machine and stretched to a certain value of strain at a specified strain rate. When the stress on the specimen reaches a constant value the test is terminated.

2.2.1.1 Obtaining the stress relaxation curves

Stress relaxation curves are plots of elasticity modulus versus time. They are plotted independently for different temperature and strain rate combinations. Performing several tests at each combination would be better in order to minimize errors.

2.2.1.2 Fitting Prony series to stress relaxation curves

Solid propellants are generally treated as generalized Maxwell materials. Therefore, as can be seen in section 2.1.6.4 the stress relaxation behaviors of the solid propellants are commonly determined as Prony series.

Fitting Prony series to the stress relaxation curves obtained by tests render smooth relaxation curves. Master curves are well represented with these smooth curves. Prony series can be represented as follows:

$$E(t) = E_\infty + \sum_{i=1}^{n} E_i \exp\left(-\frac{t}{\lambda_i}\right) \tag{2.57}$$

The terms in equation 2.57 are explained in Figure 2.14.

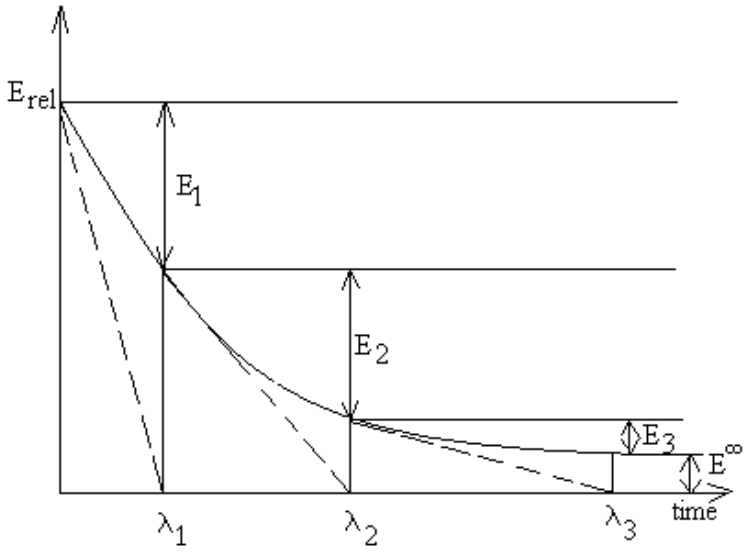

Figure 2.14: Representation of Prony series

2.2.1.3 WLF shift function and obtaining the master curve

Master curve is constructed such that the relaxation curve at the reference temperature, generally taken as the room temperature (25^{o}C), is held constant and all other relaxation curves of different temperatures are shifted among the log-time axis to form a single curve around the reference curve [1]. The amount of shift along the log-time axis is the log shift factor $log(aT)$ for that particular temperature. As mentioned in section 2.1.7 the underlying assumption that allows us to define relaxation curves at the reference temperature with shift factors is the thermoreologically simple material assumption.

The procedure of finding the shift factors requires plotting all the relaxation curves on a logarithmic scale and finding the horizontal distance of each from the reference line ($log(aT)$). To be able to do viscoelastic analysis, a function should be fitted to the shift factor. For solid propellants one of the most appropriate functions is the WLF shift function [1].

$$WLF(T) = \log\, a_T = \frac{C_1\left(T - T_{ref}\right)}{C_2 + \left(T - T_{ref}\right)} \tag{2.58}$$

2.2.2 Uniaxial Tension Tests,

Failure curves are very useful tools for failure analysis of the viscoelastic solids. These curves are obtained through uniaxial tension tests performed at different temperatures and different strain rates. Most important curves that are used for failure assessment are Smith failure envelope, main uniaxial stress curve, main uniaxial strain curve, and stress - reduced life curve.

Unlike the sress relaxation test the specimens are loaded until rupture in uniaxial tension tests. True stress - strain curves are obtained after these tests.

2.2.2.1 Failure Curves and Smith Failure Envelope

In failure analysis, stress and strain values are compared with the material strength values to obtain damage factors of various failure criteria. However, most viscoelastic materials, including solid propellants have differing strength values at different temperatures and dif-

ferent strain rates. Therefore, master failure curves that help determining strength values for different conditions are formed.

Just like the master relaxation curve, the master failure curves that define strength values with shift factors at reference temperature are based on the assumption of simple thermorheological material. This means that the materials strength values at a temperature and strain rate is same as the strength values at a lower temperature and a lower strain rate or strength values at a higher temperature and higher strain rates.

Main uniaxial failure curves show the maximum true stress and the strain at the maximum true stress with respect to $log(1/reducedstrainrate)$ (Figures 2.15 and 2.16).

Smith failure envelope shows the maximum true stress and strain at maximum true stress at different temperatures. Left side of the Smith failure envelope is the safe region (Figure 2.17).

2.2.2.2 Cumulative Damage Parameters

The environmental loads during transportation and storage of solid propellants cause stresses and strains. These stress and strains cause accumulating damage in the propellant. Concepts of damage can be integrated into viscoelastic constitutive theory [1, 12]. Cumulative damage methods are commonly used to evaluate structural integrity or service life of solid propellants. The basis of this analysis is Miner's cumulative damage rule that assumes structural failure to be the result of incremental failures that progress cumulatively as a function of the applied loads [14].

$$D = \sum_{i=1}^{n} D_i = \sum_{i=1}^{n} \frac{\Delta t_i}{t_{fi}} \tag{2.59}$$

This expression relates the cumulative damage to incremental damages D_i. In the expression 2.59 incremental damage D_i, is the ratio of time Δt_i that the specimen is exposed to the i^{th} stress level σ_i relative to the mean time to failure t_{fi} when the specimen is subjected only to σ_i. Therefore, mean time to failure must be related to applied stress level. For this purpose Bills[15] postulated the following expression.

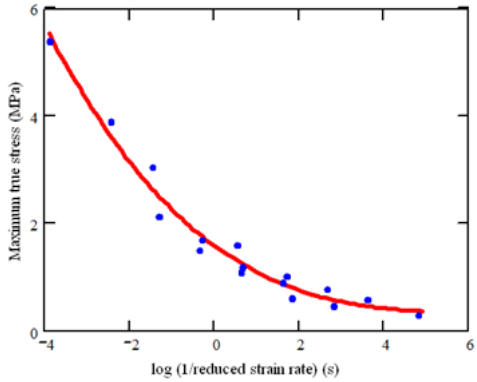

Figure 2.15: Maximum true stress

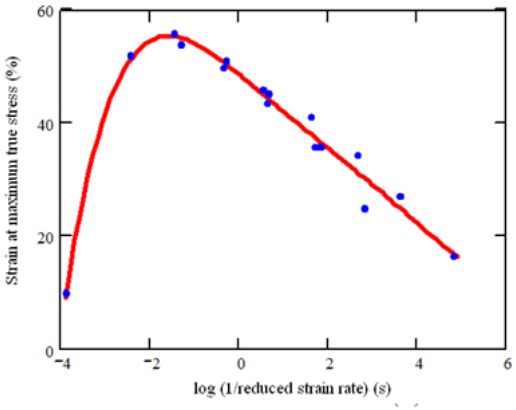

Figure 2.16: Strain at maximum true stress

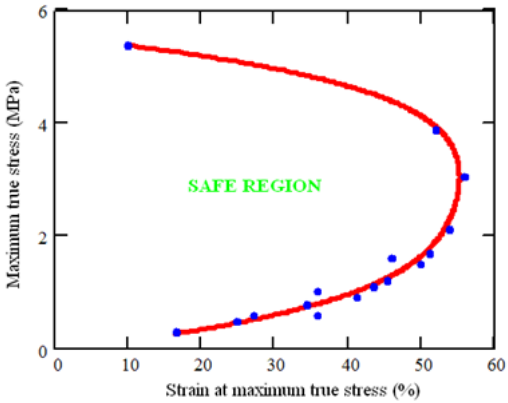

Figure 2.17: Smith failure curve

$$t_{fi} = t_0 a_T(T_i) \left(\frac{\sigma_0}{\sigma_i} \right)^{\beta} \tag{2.60}$$

Here, t_{fi} is time to failure at stress σ_i, t_0 is time to failure at reference stress σ_0, β is the negative inverse slope of the log-log plot of stress versus failure time, and $a_T(T_i)$ is the shift factor at temperature T_i Eliminating t_{fi} from 2.59 and 2.60 results in a cumulative damage expression in terms of discrete stress states.

$$D = \sum_{i=1}^{n} \left[\frac{\Delta t_i}{t_0 a_T(T_i)} \left(\frac{\sigma_i}{\sigma_0} \right)^{\beta} \right] \tag{2.61}$$

For continuous stress histories equation 2.61 can be generalized as

$$D(t) = \frac{1}{t_0 \sigma_0^{\beta}} \int_0^t \frac{\sigma(t)^{\beta}}{a_T(t)} dt \tag{2.62}$$

A simpler form of the cumulative damage expression can be obtained by taking t_0 as 1 and calculating σ_0 accordingly. In other words such a reference stress shall be chosen that failure would occur in unit time. Note that reference stress is calculated at the reference temperature.

The cumulative damage model seen in equation 2.62 has two parameters that need to be identified. These parameters, β and σ_0, can easily be obtained from log-log stress versus reduced life curve. This curve is potted with the maximum true stress value and the reduced time that it takes to reach to the maximum true stress (2.18).

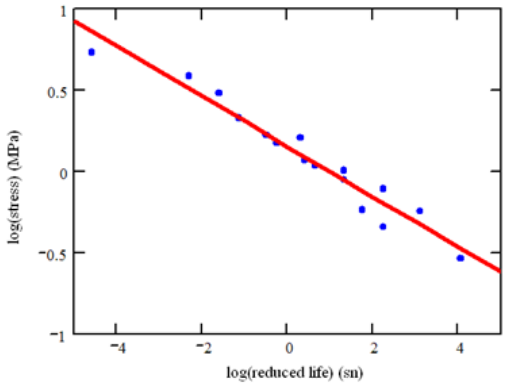

Figure 2.18: Maximum true stress versus reduced life

Let the equation of the line fitted to the data be $f(\lambda)$. β is inverse reciprocal of the slope of the line fitted to the data.

$$\beta = \frac{-1}{\frac{d(f(\lambda))}{d\lambda}} \tag{2.63}$$

Here λ is log-reduced life. σ_0 is the maximum stress value where reduced life is 1 and therefore log-reduced time is 0.

$$\sigma_0 = 10^{f(0)} \tag{2.64}$$

2.3 Service life of solid propellants

In this section, major studies made on service life of solid rocket motors are reviewed. There are many studies in the literature dealing with viscoelastic behavior of the solid propellants, their response to cyclic temperature variations, service life prediction methods, and finite element analysis of solid propellants.

Solid propellant motors are stored in many different configurations. They are frequently kept under unprotected conditions; hence they are subjected to varying thermal stresses and material degradation due to aging and fatigue.

One of the first probabilistic studies on solid propellant failure under environmental conditions is conducted by Heller et al [17]. They defined probability of failure due to environmental conditions as the probability that the thermal stress exceeds the strength of the propellant.

After statistically analyzing 10 years of hourly temperature data Heller proposed that environmental temperature is a pseudarondom variable that consists of the sum of two narrow-band excitations, whose amplitudes and frequencies have statistical variations [17] (see Figure 2.19).

Applying the proposed temperature profile to a simple elastic, hollow cylindrical propellant model, Heller, devised a propellant life prediction method. This study also shows that the probability of failure of the propellant grain under environmental temperature cycles varies

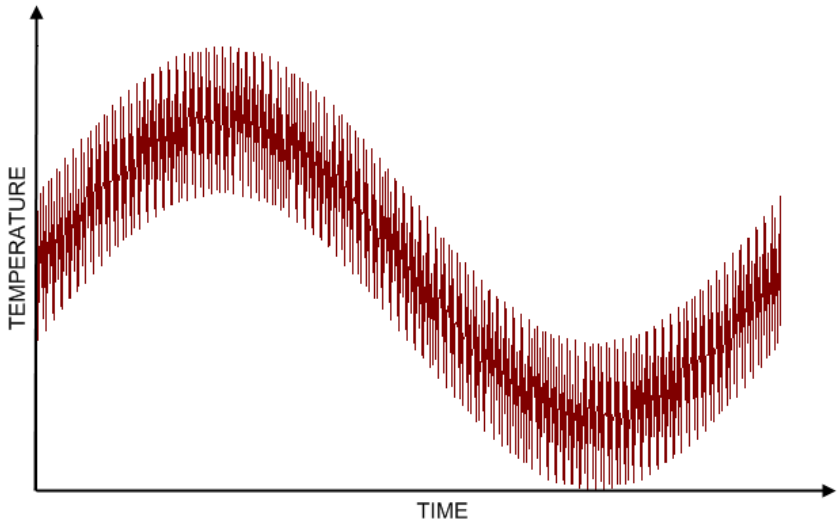

Figure 2.19: Theoretical cyclic temperature

with time and probability of failure due to excessive bore stress is much higher than other failure types.

Heller and Singh then introduced viscoelasticity to the methods they proposed in previous study [18]. In the later study they also utilized the cumulative damage methodology as an aging model for the propellant depending on the results of experiments performed by Bills [16]. These experiments indicate that the linear cumulative damage rule may be useful in the prediction of solid propellant service life.

In another study, Heller, Singh and Zibdeh focused on cumulative damage of the viscoelastic solid propellant and showed that time-temperature shift characteristics of the solid propellant may sometimes dominate over stress level. Contrary to intuition, greater damage may be produced even though the stress is lower at relatively high temperatures [19].

Thangjitham and Heller made further investigations on temperature and stress distributions in solid propellant rocket motor exposed to environmental thermal loads [20]. Their findings show that in the absence of solar radiation, surface temperature is very close to air temperature.

In another study, Zibdeh and Heller discusses the first passage method in service life predictions for solid rocket propellants utilizing cumulative damage concepts and chemical aging [21]. Their results show that cumulative damage is much more effective in reducing the

strength then aging. The effect of aging can be neglected whereas cumulative damage may reduce the strength dramatically.

Another study emphasizing the importance of cumulative damage and time-temperature shift properties of the viscoelastic propellant material is carried out by Margetson and Wong [22]. In their study they managed to incorporate these concepts with measured stress data for service life prediction of solid rocket propellants.

Chen and Leu made finite element analysis to obtain the response of the solid propellant under cyclic thermal loads [23]. They utilized linear viscoelasticity in their analysis and later validated the results with experiments.

Duncan and Margetson developed a uniaxial nonlinear viscoelastic constitutive equation incorporating cumulative damage for solid rocket propellants [12]. Their nonlinear components included strain rate and cumulative damage terms. They calibrated the cumulative damage parameters with two experiments performed at opposing extreme values of strain rate. They also give comparisons of linear viscoelastic results and experimental stress data.

Chyuan investigated temperature history effect for viscoelastic solid propellant grains. Their findings show that the thermal loading history effect is important for structural integrity of solid propellant grains [24]. He also discusses that in general, the critical location under the ignition pressurization loading case is at the bond-line interface between the motor case and propellant, and the critical location under thermal loading is the inner bore surface.

Akpan and Wong provide an example of probabilistic approach to service life assessment of solid rocket motors [25]. They also investigated the most effective parameters on the solid propellant service life through sensitivity analysis. Their findings show that the propellant capacity (strength) which reduces with accumulated damage and thermal expansion coefficient are the most effective factors.

CHAPTER 3

PARAMETRIC GRAIN MODEL

Geometry of the grain is one of the most commonly changing parameters in the design procedure. While studying phenomena that highly depend on geometry of the grain such as propellant storage life, it is very useful to have the ability to parametrically generate finite element models of the grain as the geometry changes.

Such a tool not only enables optimization of the geometry against conflicting requirements but it also provides interoperability of the methods applied during a geometry dependent study.

In harmony with the problems at hand, a parametric finite element model generator for the finocyl type of grains was developed.

Grain types other than finocyl can also be implemented in such a parametric geometry generator. This would require careful parameterization of the grain type and implementation of the codes that would generate the geometry.

The following sections describe in detail the geometric parameters of the finocyl grain and generation of the finite element mesh.

3.1 Geometric parameters

Finocyl is a very commonly used type of grain geometry and it's not a very simple geometry for modeling. It has many features resulting from different requirements of structural integrity or ballistic performance. An automated finocyl geometry generation tool should be able to handle many aspects of the geometry.

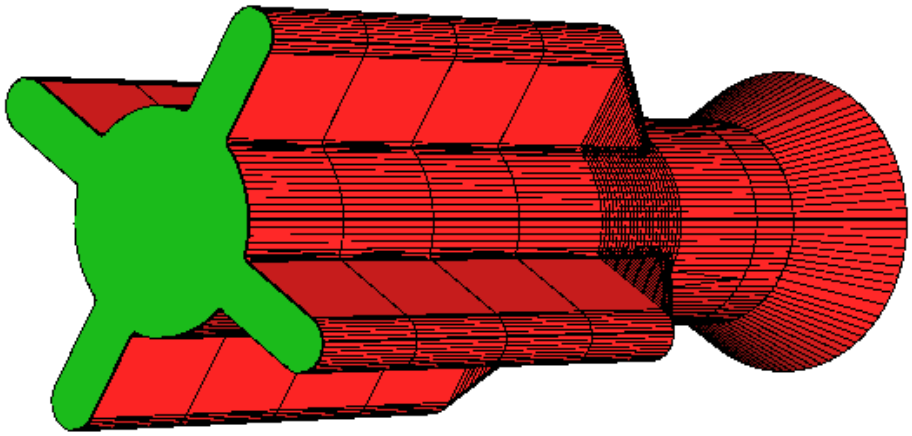

Figure 3.1: Finocyl grain, surface mesh of the bore

Figure 3.1 shows the surface mesh of the conduit of a typical finocyl grain generated by the geometry generation tool developed in this study (GrainPar). GrainPar is an automatic propellant grain geometry generator developed in Borland Delphi. The finocyl geometry seen in Figure 3.1 is a 4 armed finocyl grain designed by GrainPar. The surface mesh of the one eighth of solid propellant grain for the same geometry is illustrated in Figure 3.2.

Figure 3.2: Finocyl grain partial surface mesh

As Figures 3.1 and 3.2 may imply, finocyl geometry is not a simple geometry. Number of geometric parameters used in GrainPar to model the finocyl is 34. These geometric parameters, explained in sections starting from 3.1.1, together with 9 parameters defining the fineness of the surface mesh, dictate the geometry generated by GrainPar.

It is meaningful to examine the finocyl geometry in six sections along its longitude. Starting

from the back, first of these sections is the aft stress relieving section or the aft cap of the grain. The following section is the fin conduit where the fins lie all along the section length. Fin to circular conduit transition section is between the circular and fin conduit sections. After the circular conduit section, come the diverging section and the fore cap (Figure 3.3).

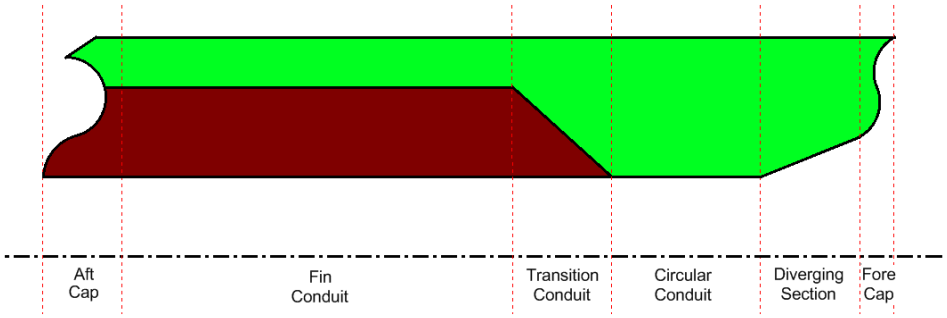

Figure 3.3: Finocyl grain sections along its longitude

Each section described above has its own set of parameters defining its geometry in GrainPar. This feature provides extra flexibility to GrainPar and enables easy implementation of other configurations of finocyl grain or a totally different grain geometry with similar section profiles.

It must be noted that, at its current state GrainPar only supports finocyl grains. Finocyl grain geometry is one of the rather complex geometries of grains. Therefore, finocyl grain, being used commonly in real rocket applications, was chosen as a starting point for the development of GrainPar.

3.1.1 Number of Arms (Narm)

Number of Arms defines the number of fins existing in the fin conduit and transition sections of the finocyl grain. Number of finocyl arms may vary throughout the design for ballistics or structural reasons.

Number of arms also affect the structural finite element analysis of the grain. For consistently symmetric loads, only a portion of the full model is required for the finite element analysis. For pure thermal loads this is only a portion consisting of the one half of an arm and its surrounding. Hence, for a four armed finocyl grain, one eighth of the full model is required,

whereas a six armed finocyl grain would only require one twelfth of the model (Figure 3.4).

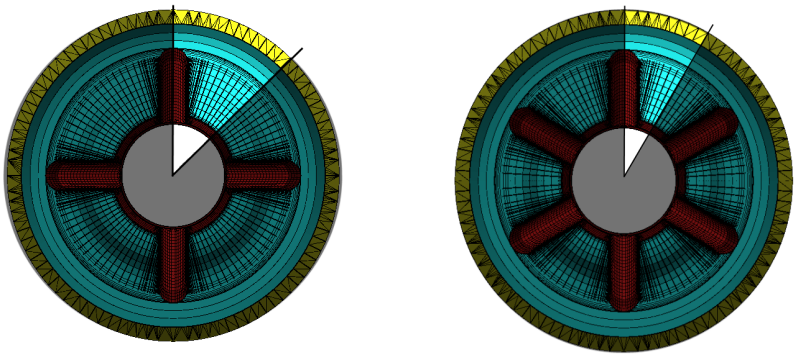

(a) 4 armed finocyl (b) 6 armed finocyl

Figure 3.4: Finite element analysis sections for symmetric loading case

However, when the loading case is not symmetric as explained above, the full model may be required. GrainPar can produce finite element meshes for both cases.

3.1.2 Section Inner Radius Profile (ainr, binr)

There are four sections in the GrainPar's finocyl model that needs a linear profile to be defined. These four sections are the all conduit sections including the diverging section. These profiles can be defined separately, generating step changes between the sections, or they can be defined in unison to create a continuous profile.

In composite solid propellants the inner bore is designed to have slightly changing radius along its longitude, this is to provide ease of removal of the mandrel after the curing process. Together with this, for ballistic performance optimization, designer may chose to have differing bore inner radiuses.

Inner bore radius within a section of the grain is defined as a linear function in GrainPar:

$$inr(x_{\text{sec}}) = a_{inr} x_{\text{sec}} + b_{inr} \tag{3.1}$$

Where x_{sec} is the distance from the beginning of the section. a_{inr} and b_{inr} are the function parameters defined for each section (Figure 3.5).

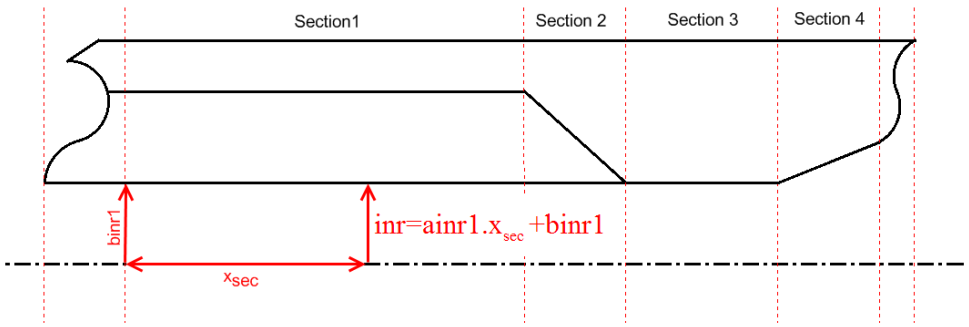

Figure 3.5: Finocyl inner radius parameters

The parameters a_{inr1} and b_{inr1} seen in Figure 3.5 are defined only for section one. The number "1" defines the section that this parameter belongs to. To define the inner radius profile of section two, a_{inr2} and b_{inr2} are used. There are similar parameters for sections three and four.

3.1.3 Arm Height Profile (aharm, bharm)

Arm height profile is defined similar to the inner radius profile. Since fins only exist in sections designated as 1 and 2 in Figure 3.5, only these sections require arm height profile definition.

In most of the finocyl designs, fins exist only in a portion of the grain length. Fins generally disappear gradually through a transition section as seen in section 2 of Figure 3.5. However, it is possible to have grain geometries where fins disappear immediately.

For better understanding of the fins or arms of the finocyl grain design, a cross section of a finned grain is illustrated in Figure 3.6.

3.1.4 Arm Width (Armw)

Arm width defines the width of the arm in GrainPar. This parameter also sets the diameter of the half circle located at the top of the fin (Figure 3.6).

Care should be taken when setting the value of arm width, since it also limits the number of arms that can be defined. Wide arms with high number of arms will cause errors in surface mesh generated by GrainPar. For example, consider a grain with 8 arms that has a constant

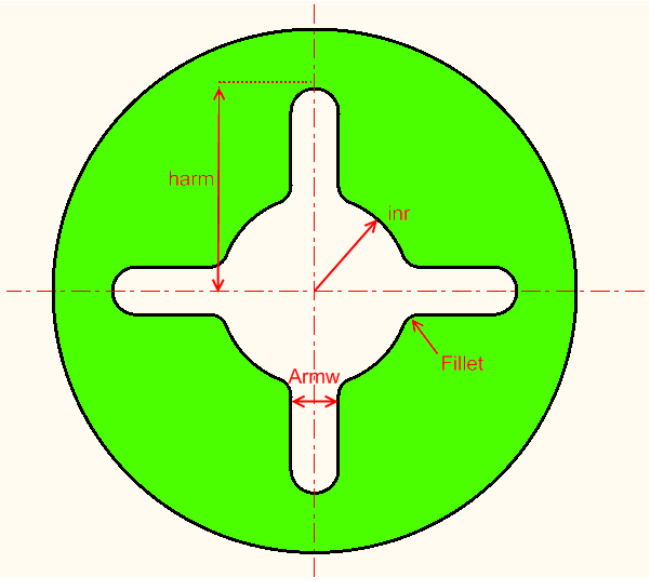

Figure 3.6: Finocyl cross section

inner radius of 80. If arm width of this propellant grain is chosen to be 80, it would be impossible to create 8 arms of such width since the arms would overlap.

3.1.5 Fillet Radius (fillet)

This parameter sets the radius of the fillet lying between the root of the fin and the inner circular portion of the cross section (Figure 3.6). Fillet radius should also be chosen with care since it can lead to surface mesh errors in case of an inconsistency with the sections inner radius or arm height profile.

Too small values of the fillet radius will produce adjacent nodes in the final surface mesh since GrainPar tries to place a certain number of nodes along the fillet. This can be corrected by changing the number of nodes placed along the fillet (see section 3.2) or by using mesh refinement utilities of the GrainPar.

3.1.6 Section Lengths (Lsec)

The four sections seen in Figure 3.7 require their lengths to be specified in GrainPar. Section lengths of the finocyl grain are some of the most important parameters dictating the ballistic

performance of the solid propellant motor. These section lengths are varied throughout the design process to optimize the ballistic performance of the rocket motor. Therefore, sufficient flexibility shall be provided by the grain geometry generator.

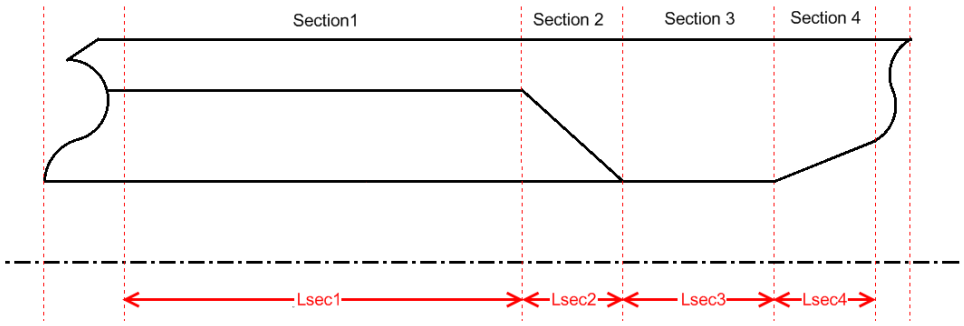

Figure 3.7: Section lengths

Section inner radius and arm height profiles highly depend on the section lengths, especially for continuous profiles. Parameterization of these profiles should be done in consistency with the specified section lengths. An arm height profile example is shown in Figure 3.8. The parameters required to produce the profile shown in Figure 3.8 are listed in Table 3.1.

3.1.7 Aft Cap Parameters (acrad, acz, acr)

Aft cap or the aft stress reliever section of the finocyl grain is modeled as two intersecting arcs in GrainPar. Stress reliever design carries importance for structural integrity of the propellant. The propellant grain is exposed to very high pressures during ignition and burnout. The stress reliever design is optimized to reduce stress concentration points in the propellant.

The two arcs that form the aft cap are defined with the relative positions of their centers from the centroid of the motor and the beginning of the first section (Figure 3.9) and their radiuses.

The stress reliever arc closer to the centroid of the motor is denoted as ac1 and the one farther away is denoted as ac2. Hence, acrad1 defines the radius of the arc ac1. acr1 is the radial distance of ac1's center to the centroid of the motor and acz1 is the position of the arc's center in z axis relative to the beginning of section1 (Figure 3.9). Same convention applies for the second aft cap arc ac2

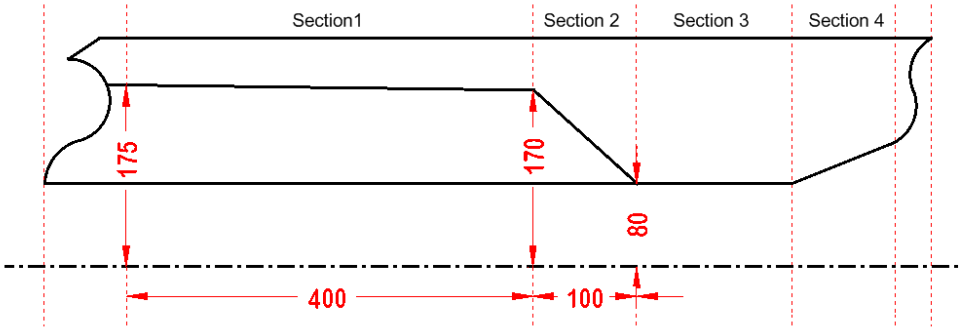

Figure 3.8: Arm height profile example

Table 3.1: Parameters for arm height profile example

Section	Parameter	Value
	Lsec1	400
1	aharm1	-0.0125
	bharm1	175
	Lsec2	100
2	aharm2	-0.9
	bharm2	170

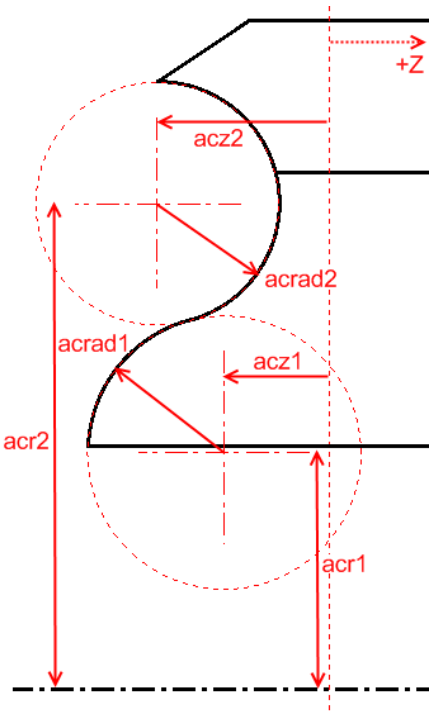

Figure 3.9: Aft cap

3.1.8 Fore Cap Parameters (fcrad, fcz, fcr)

Fore cap is also designed as two intersecting arcs in GrainPar. Definition of these arcs are realized as the aft cap arcs. However, in the case of fore cap arcs, although fcr defines the radial distance from the motor centroid, fcz is the relative position of the arc in z axis from the end of the fourth section (Figure 3.10).

3.1.9 Outer Shell Radius (outr2)

Outer shell radius is the radial distance of the outermost surface of the grain from the motor centroid. This distance can be seen in Figure 3.10. This surface is also called the propellant-case bond line.

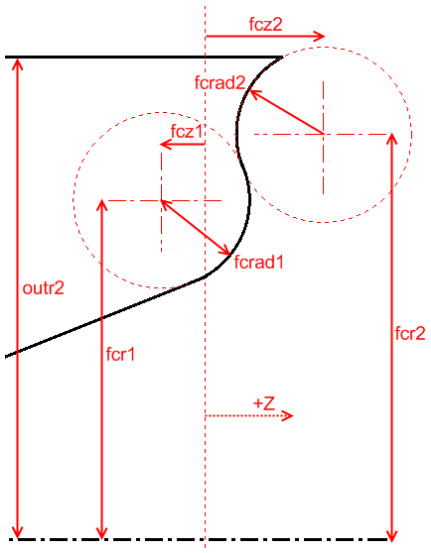

Figure 3.10: Fore cap

3.1.10 Cut section parameters (outr1, Lcut)

Cut section is located in the foremost section of the motor where it interfaces with the stress reliever. Case and the propellant grain are generally separated further away from each other in the cut section and the resulting vacancy is filled with thicker insulator material.

As seen in Figure 3.11, cut section is defined by two parameters. outr1 is the radial distance of the cut section and fore cap interface from the motor center line and Lcut is the projection of the cut section length in z axis.

3.2 Surface Mesh Properties

As mentioned before, besides the parameters defining the geometry of the grain, there are also parameters that need to be defined for mesh fineness of the GrainPar output. There are 9 parameters in GrainPar to generate the surface mesh of the grain.

These parameters are explained in detail in Table 3.2. Care should be taken when major changes are made on the geometric parameters of the grain since some of the mesh properties depend on geometric parameters. The parameters *sbigarc* and *ssmallarc* for example, define the number of lines that the related arc will be divided into. If the arc radius is increased, the

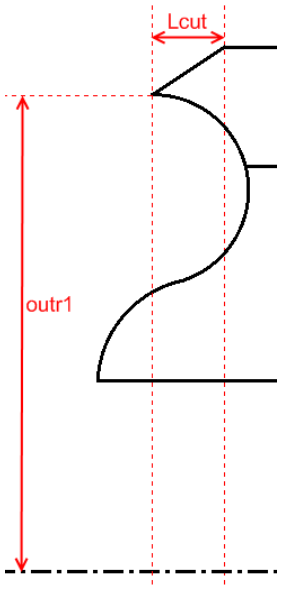

Figure 3.11: Cut section

number of divisions should also be increased consistently.

3.3 Solid Mesh Generation

GrainPar generates the surface mesh of the solid propellant grain. However, for finite element method to be used for structural analysis, a 3D solid mesh of the grain is required. Since the surface of the grain geometry is already constructed boundary conformity mesh generation technique is used to obtain the solid mesh of the grain.

As explained in previous sections, the solid propellant grain has very complicated geometric features. These features generally lead to use of tetrahedral meshes. Tetrahedral solid mesh of the solid propellant grain is obtained through Delaunay[1] tetrahedralization and quality mesh generation.

Tetrahedralization of the grain geometry is realized by an open source computer code called TetGen. TetGen is a powerful tool for decomposing an arbitrary 3D piecewise linear complex into a constrained Delaunay tetrahedralization. A piecewise linear complex (PLC) is representation of a 3D geometry by vertices (points), edges defined between vertices and facets

[1] Soviet/Russian mathematician Boris Nikolaevich Delaunay (1890 - 1980)

Table 3.2: Surface mesh parameters

Parameter	Explanation
nfillet	This parameter defines how many nodes will be used in modeling the fillet section of each grain slice.
sbigarc	This parameter defines the number of equally sized angular portions a 90 degree segment of the inner bore will be seperated into.
ssmallarc	This parameter defines the number of equally sized angular portions a 90 degree segment of the arc at the top of a fin will be seperated into.
dz	This parameter defines the distance between the slices of the grain taken along the longitude except the transition section.
dz2	This parameter defines the distance between the slices of the grain taken along the longitude in the transition section.
nfilletless	This parameter defines how many nodes will be used in the interface between fin top and inner bore for the model of the slices in transition section where the fin has sinked below the fillet level.
fcdr	This parameter is the maximum radial distance of the projection of the fore cap nodes in xy plane.
acdr	This parameter is the maximum radial distance of the projection of the aft cap nodes in xy plane.

composed of these edges. The surface mesh generated by GrainPar is a typical example to a PLC. Methods for constrained Delaunay tetrahedralization is discussed in detail by the author of TetGen[2] in reference [26]

For a three-dimensional domain, defined by its boundary (such as a surface mesh), TetGen generates the boundary constrained Delaunay tetrahedralization, conforming Delaunay tetrahedralization, quality Delaunay mesh [28]. Tetrahedral mesh of the grain geometry shown in Figure 3.2 generated by TetGen can be seen in Figure 3.12. Another view of the same geometry from a cut plane can also be seen in Figure 3.13.

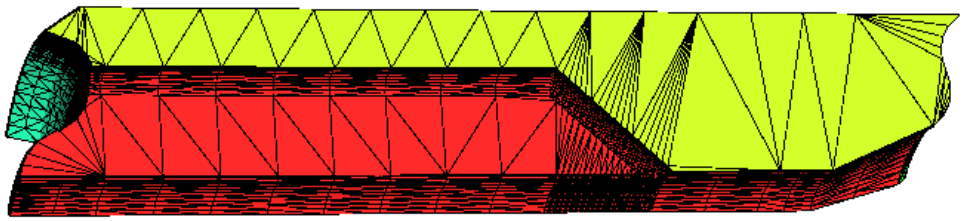

Figure 3.12: Tetrahedral mesh

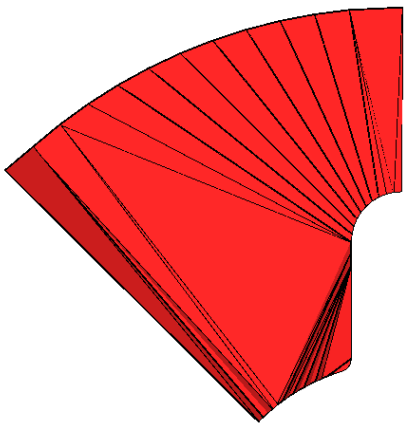

Figure 3.13: Tetrahedral mesh, cut plane view

The next step in obtaining the quality mesh of the grain is to refine the initial mesh obtained through Delaunay tetrahedralization. Being aimed at generating meshes for finite element method or finite volume method, TetGen also provides methods for refining the mesh by introducing constraints to shape and size of the elements.

[2] Hang Si, Weierstrass Institute for Applied Analysis and Stochastics, Berlin, Germany

Delaunay refinement is accomplished by adding new vertices to the mesh and splitting the tetrahedral. The major parameter indicating the quality of a Delaunay mesh is the radius-edge ratios of the tetrahedral in the mesh. However, this parameter cannot indicate slivers which are among the most severe tetrahedral mesh problems. Slivers are very flat, almost degenerate tetrahedral. TetGen's refinement algorithms can also avoid slivers efficiently. Hang Si explains Delaunay refinement in reference [27].

The quality meshes generated after refinement of the meshes seen in Figures 3.12 and 3.13 are presented in 3.14 and 3.15.

GrainPar is configured to be fully compatible with TetGen and its utilities. PLC files can directly be generated and TetGen can be run directly from GrainPar. Resulting meshes can be viewed from GrainPar by an external mesh viewer called TetView. Mesh quality and size parameters can also be controlled directly from GrainPar.

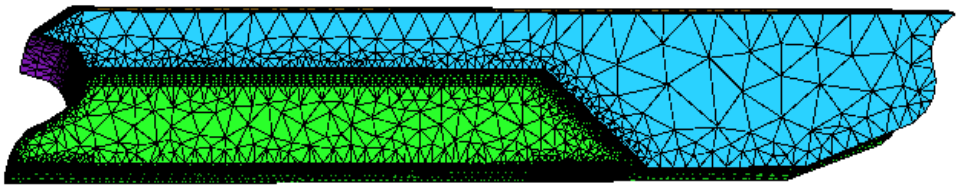

Figure 3.14: Refined tetrahedral mesh

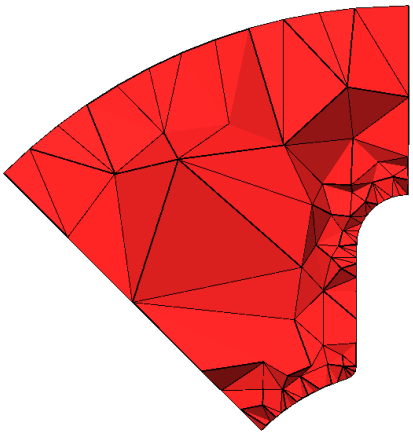

Figure 3.15: Refined tetrahedral mesh, cut plane view

CHAPTER 4

FINITE ELEMENT ANALYSIS

Responses of the solid propellant grain to the thermal effects are modeled in this study by finite element analysis (FEA).

Finite element analysis, sometimes referred to as the finite element method, relies on mesh discretization of a continuous domain for solving complicated partial differential equations or integral equations. The development of FEA can be traced back to 1940s where Alexander Hrennikoff[1] and Richard Courant[2] developed mesh discretizations for solving problems in continuous domain.

The finite element analysis performed for characterization of strain-stress response of the grain to temperature profiles applied to the case of the solid rocket motor can be performed in two steps.

First step in performing FEA for this purpose is to investigate the temperature response of the grain through thermal analysis. The second step is to apply the temperatures found in the first step to the structural FEA to investigate the strain-stress response of the propellant grain.

This two step approach may be called a coupled field analysis where combinations of different types of analyses interact to solve a problem that concerns more than one physics field. Therefore, if an analysis has inputs that need to be determined by another analysis, these analyses are coupled.

The coupling of two analyses may be one way or two ways. In the latter one, both analyses have factors that depend on the other. However, in cases like thermal stress as in this study, the

[1] Russian-Canadian Structural Engineer (1896-1984)
[2] German-American Mathematican (1888-1972)

coupling is one way. The temperature profile causes thermal strains that affect the structural analysis where the structural strains or stresses generally have no effect on temperature.

One way coupled analyses are easier to handle since the analyses can be run in turns to obtain the final results. However, solution of two ways coupled analyses requires iterations between the coupled fields.

Both thermal and structural finite element analyses are carried out in ANSYS software package in this study. ANSYS provides powerful batch operation options, highly parameterized finite element models, and easy interaction with external applications through ANSYS Parametric Design Language (APDL). Although the analyses carried out in this study are one way coupled, ANSYS can also manage two ways coupled analyses. ANSYS also incorporates structural and material nonlinearities, making it favorable for a very wide range of problems.

GrainPar is configured to be easily coupled with ANSYS, allowing direct export of the meshes generated by TetGen to ANSYS and preparation of APDL input files for both thermal and structural analyses. Any finite element analysis tool that has the ability to import meshes and allows batch input can be configured to work with GrainPar. Figure 4.1 illustrates the steps of the finite element model generation.

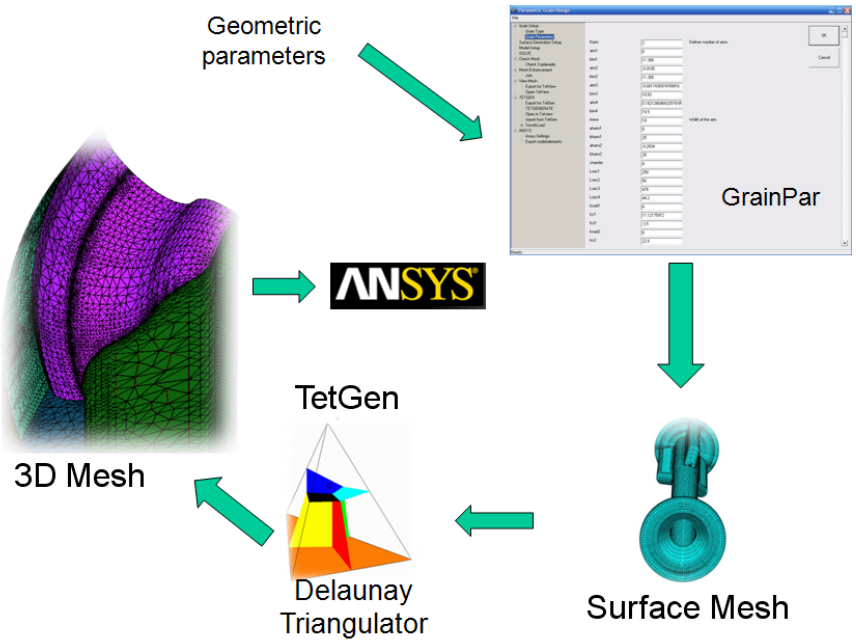

Figure 4.1: Finite element model generation

4.1 Element Selection, Material Models, and Material Model Verification

There are many element options to choose from in ANSYS. For a viscoelastic structural analysis to be realized the element chosen should support viscoelastic material models. Furthermore, since tetrahedral meshes created by TetGen are directly imported to ANSYS the element should also be able to allow for tetrahedron shape. Care should be taken since not all elements which allow tetrahedron shape are recommended to be used in their tetrahedron form.

For the case of structural analysis, Solid187 element of ANSYS satisfies the requirements listed above. Solid187 is a ten-node tetrahedral structural solid element which has mid-nodes along its edges to allow for nonlinearities.

Thermal analyses in this study are carried out in two dimensions to save from computational time. The model is generated by the input file created by GrainPar and the 2D mesh is generated by the internal meshing utilities of ANSYS. A two dimensional thermal element, PLANE55 is used for thermal analysis carried out in ANSYS. ANSYS offers a very wide range of material models which can be combined in order to represent complicated material behaviors.

Linear viscoelasticity is modeled as a combination of linear isotropic model, prony series, and shift function in ANSYS. The material model defined in ANSYS is later verified by a viscoelastic stress solver developed using the equations given in Chapter 2. The material model is given in Appendix A.

For the sake of clarity prony series representation of the relaxation function or the master curve will be briefly explained since there is a slight difference between the ANSYS representation and notation followed in previous sections.

As mentioned before ANSYS viscoelastic model contains both linear isotropic model and prony series representation. The modulus defined by the isotropic model actually combines with the prony series to form a single relaxation function as shown below:

$$E(t) = E_0 \sum_{i=1}^{N} E_i e^{-t/\lambda_i} \tag{4.1}$$

Where E_0 is the modulus defined by linear isotropic model and E_i and λ_i are relative modulus and relative time constants of prony series defined in ANSYS. As equation 4.1 implies, the prony series in ANSYS actually defines what ratio of the modulus is lost after a certain amount of time. Therefore at $t = 0$ equation 4.1 gives the modulus as $E(0) = E_0$.

To be able to perform thermal stress analysis, further properties such as thermal expansion coefficient, thermal conductivity, specific heat, and density have to be defined.

The consistency of the linear viscoelastic model constructed in ANSYS with the characterized viscoelastic properties are verified through a viscoelastic stress solver code that incorporates the concepts explained in Chapter 2. An arbitrarily chosen temperature profile (Figure 4.2) is applied uniformly to a hollow cylinder body and resulting thermal strains at an arbitrarily chosen location are found through FEA. The resulting thermal strains at this location can be seen in Figure 4.3. The temperature profile and the strains are input to the viscoelastic stress solver to calculate the resulting stress. Afterwards the stress results of ANSYS and linear viscoelastic code are compared to verify the ANSYS material model. As seen in the figures 4.4 and 4.5, the stress findings of these two are fully compatible.

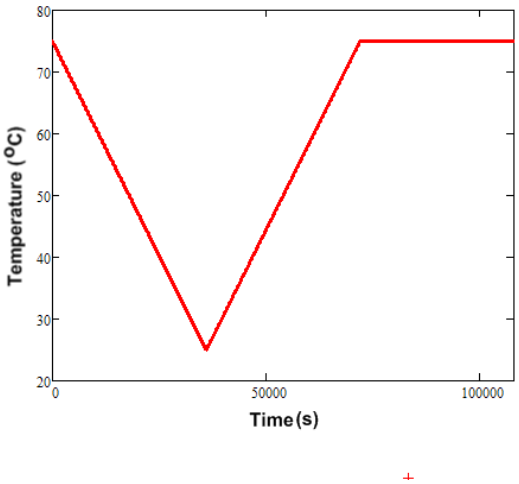

Figure 4.2: Temperature Profile

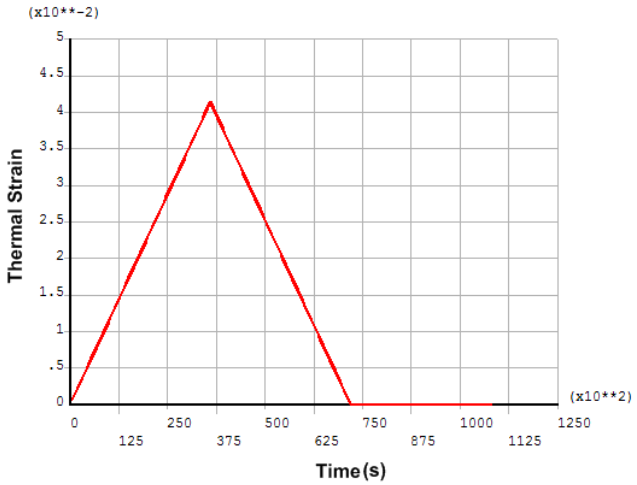

Figure 4.3: Thermal Strain

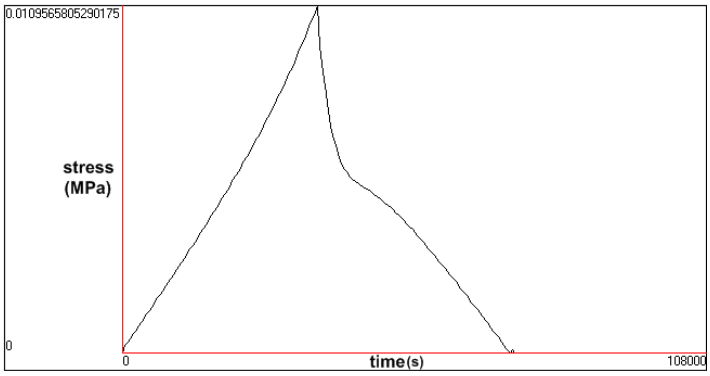

Figure 4.4: Linear viscoelastic code, stress results

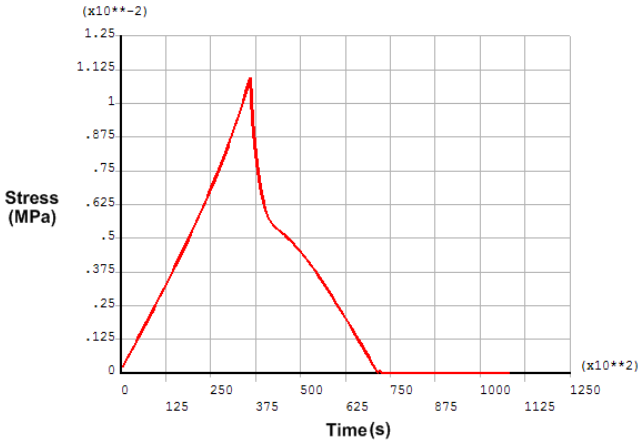

Figure 4.5: ANSYS stress results

4.2 Thermal Analysis

Thermal analysis are performed in order to discover the time dependent temperature field within the propellant grain resulting from changing case surface temperatures. Being the first step of the coupled fields analyses the thermal analysis are performed in two dimensions to save from computation time.

The major assumption that simplifies the problem to a 2D thermal problem is that heat exchange occurs only on the surface of the rocket motor case.

The affects of the fins on the temperature field are investigated to develop a 2D model for thermal analysis. The one eighth model of a 4 armed finocyl grain seen in Figure 4.6 consists of the propellant grain encapsulated by the motor case and air at the innermost section. Boundary conditions for thermal finite element analysis are also depicted in Figure 4.6.

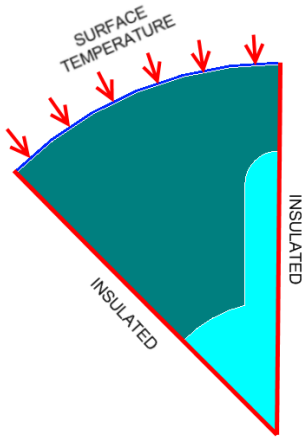

Figure 4.6: Thermal analysis model

A sinusoidal temperature cycle consistent with a daily temperature cycle is applied to the case surface and time dependent temperature fields are investigated. The findings of this analysis show that except for small deviations the temperature field can be said to have constant temperature values among a circle of constant radius (Figure 4.7). Therefore, further thermal analyses are performed by a hollow cylinder model. The temperatures of inner locations are mapped to the 3D structural model by their radial distance to the center of the motor.

Daily temperatures in this study are assumed to be sinusoidal with varying means and am-

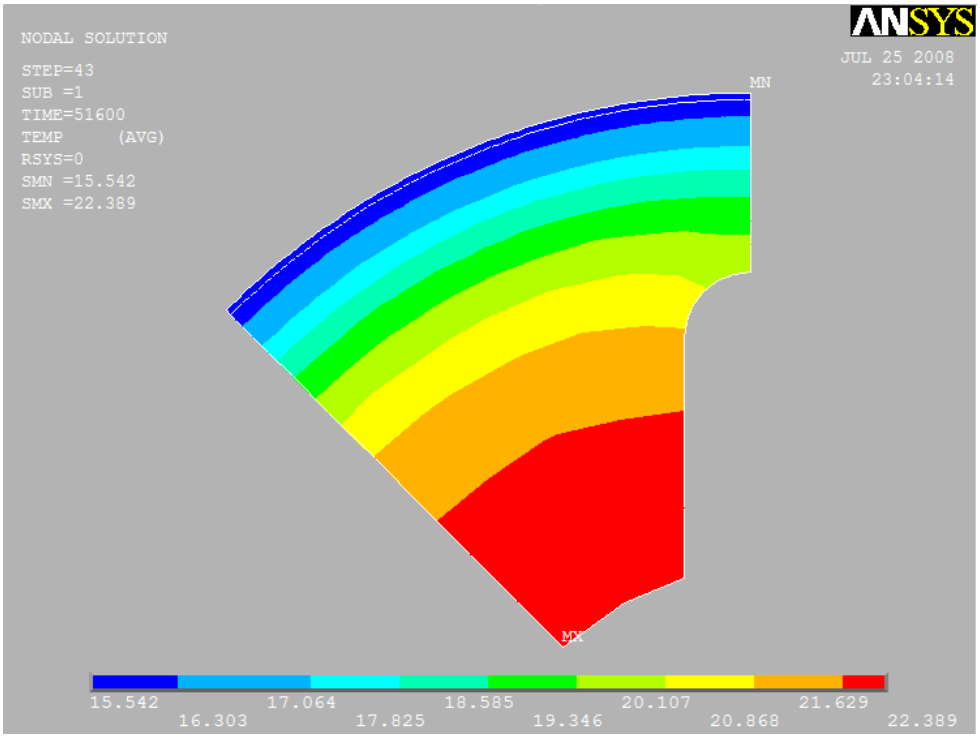

Figure 4.7: Temperature field at an arbitrary time

plitudes. A mean daily cycle for each month of the year is taken and analyses are conducted at these 12 different temperature cycles. These average daily cycles are determined from the records of Ankara from The World Meteorological Organization (WMO) of the UN (see Table 4.1).

4.3 Structural Analysis

The second and last step of the coupled-field FEA is the structural analysis. This analysis constitutes the most computationally time consuming part of the whole process due to both time dependency of the problem and complex material behavior.

Temperature fields found in thermal analysis for each time increment is applied to the propellant grain in consistent time steps to analyze strains and stresses in the material. Since the failure criteria to assess the structural integrity of the propellant grain in this study deals with effective stress, the illustrations in the following sections mainly show effective stress. However, this methodology can readily be used for assessing any failure criteria depending

Table 4.1: Climatological Information of Ankara (WMO data)

Month	Mean Temperature °C Daily Minimum	Daily Maximum	Mean Total Rainfall (mm)	Mean Number of Rain Days
Jan	**-3.5**	**4.1**	**38.8**	**12.3**
Feb	**-2.8**	**5.9**	**35.1**	**11.3**
Mar	**0.2**	**11.1**	**36.7**	**10.8**
Apr	**5.1**	**17.3**	**41.8**	**11.1**
May	**9.4**	**22.2**	**51.1**	**12.3**
Jun	**12.6**	**26.4**	**33.8**	**8.6**
Jul	**15.4**	**29.9**	**14.6**	**3.7**
Aug	**15.4**	**30**	**10.9**	**2.4**
Sep	**11.3**	**25.8**	**16.8**	**3.9**
Oct	**6.8**	**20**	**25.8**	**6.7**
Nov	**2.4**	**12.9**	**31.4**	**8.1**
Dec	**-0.9**	**6.3**	**45.7**	**12.1**

on any strain or stress component.

One of the major assumptions made in structural analysis of the solid propellant grain involves the degree of freedom (DOF) constraints. Since the thermal expansion coefficient of the aluminum motor case is approximately 25% of the thermal expansion coefficient of the motor case, the propellant is assumed to be fixed along the interface. This assumption allows the structural analysis to be performed with only the propellant material simplifying the model considerably and saving computational time. This approach can be considered conservative since if the case material was also modeled and included in the analysis, the stresses would have been slightly lower than what is found in this study. However, this methodology presented has the ability to include these complexities for further studies. It must be noted that this study deals with forming a methodology for assessing the propellant life in parametric design process. Therefore, the case study is carried out in the most economic way with limited computational power.

The boundary conditions of the structural analysis performed is presented in the cross section view of the propellant in Figure 4.8.

The other major assumption adopted in structural FEA is omission of effects of gravity which, if included, would increase the number of elements in the finite element model two folds. This increase in element number arises from changes in the symmetry condition when gravity is

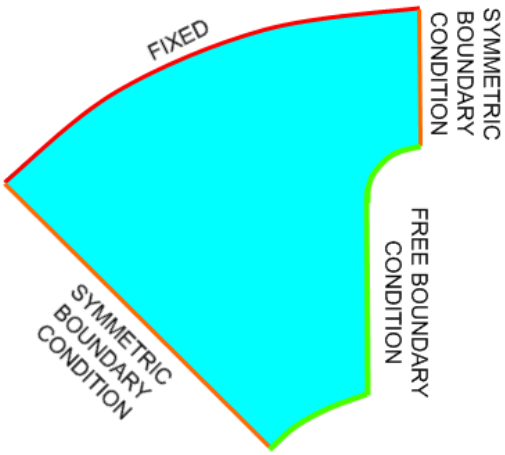

Figure 4.8: Boundary conditions

included. If gravity exists, a vertical symmetry plane passing through the center of the motor can be defined. This disables the symmetry condition as defined in Figures 3.4 and 4.8.

The effect of gravity on the solid propellant grain is evaluated with a separate analysis performed with the complete model. The results show that stresses arising from gravity are very small compared to thermally induced stresses. Furthermore, the locations of maximum stress are also different. Based on these findings, gravity effects are neglected in this study.

The contour plots illustrating stresses in the case of pure gravitational load can be seen in Figures 4.9 and 4.10. Gravitational acceleration is applied in y direction in this analysis.

The mesh used for structural analysis is generated by TetGen (see Figure 3.14) and migrated to ANSYS by GrainPar after necessary conversions are made. GrainPar is capable of generating an APDL input file, a nodes file, an elements file, and list files for boundary conditions. This capability allows directly running ANSYS in batch mode.

GrainPar also reads the output file of the thermal analysis and embeds the temperature fields found into the structural analysis APDL input file. Therefore, coupling of two different analyses in different domains are accomplished by GrainPar.

Daily temperature changes are assumed to be sinusoidal and are chosen for each month according to table 4.1. As expected, resulting stresses are also cyclic in nature. However, due to unknown initial state, solving a single cycle is not sufficient since it takes some time be-

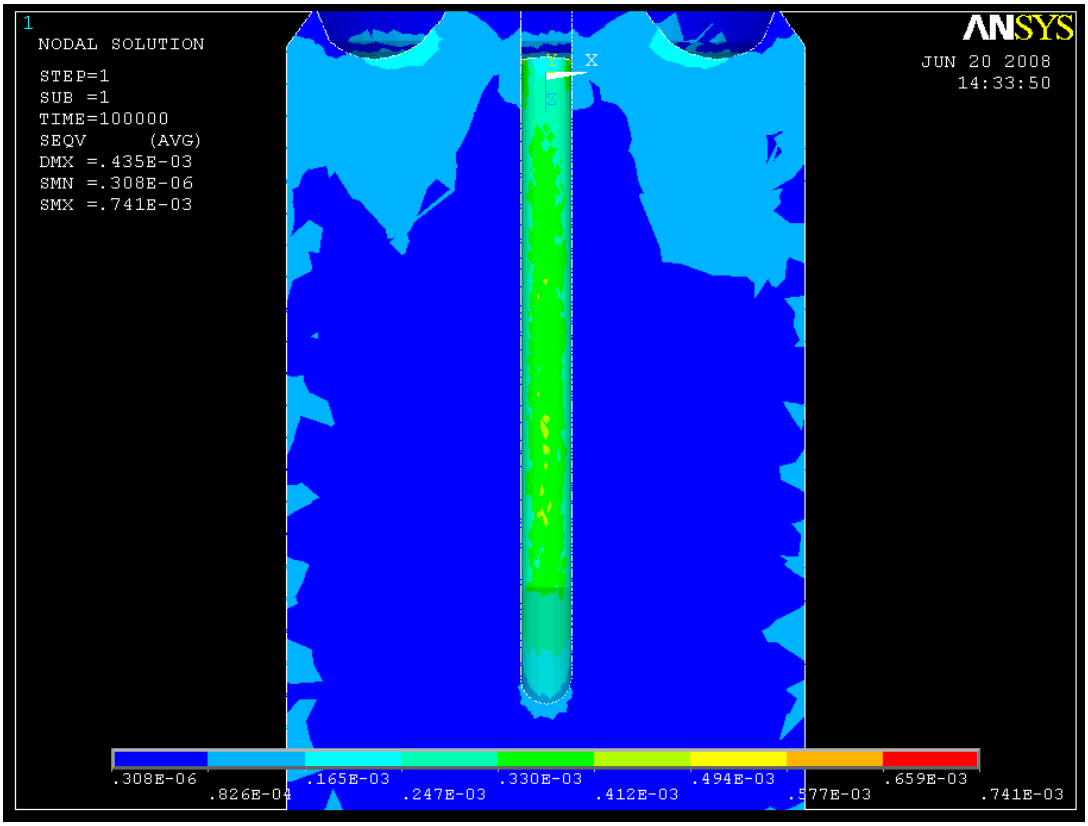

Figure 4.9: Gravitational stress field, XZ plane view (MPa)

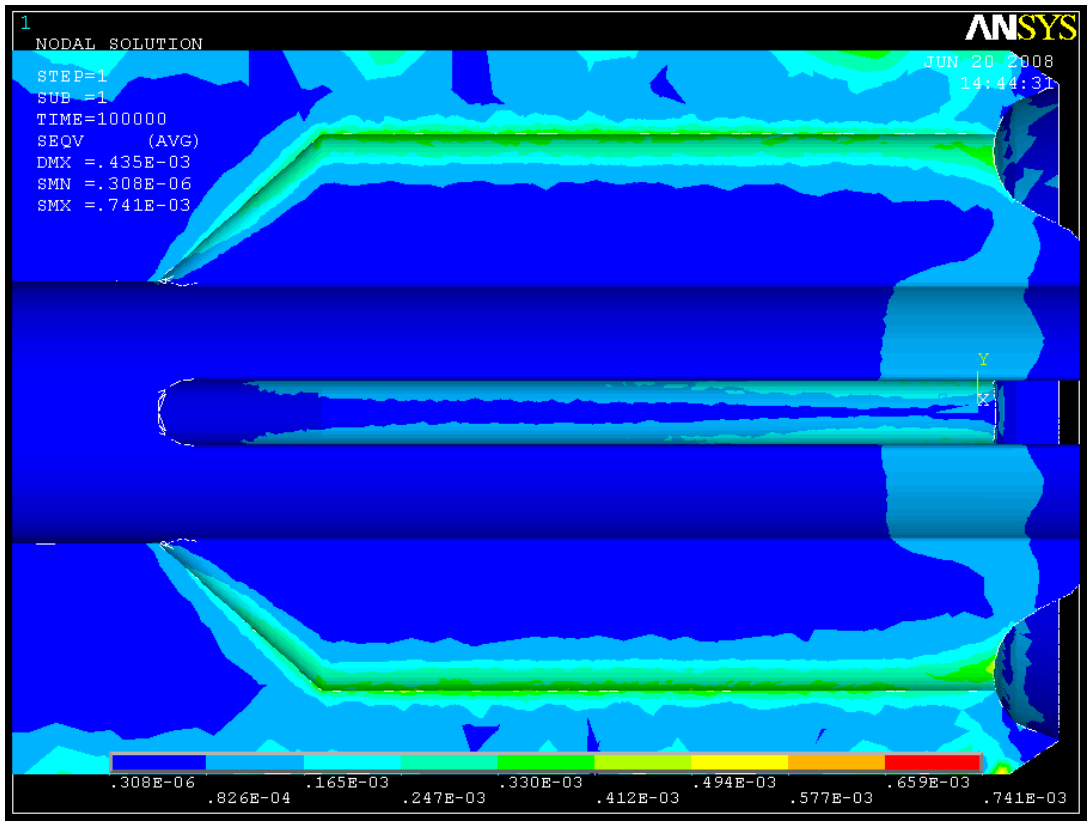

Figure 4.10: Gravitational stress field, YZ plane view (MPa)

fore the stress settles into consistent cycles. This behavior can be seen in Figure 4.11 which illustrates the FEA effective stress results for the node of maximum stress for January cycle. Figure 4.12 shows stress field for an arbitrary time of the same analysis.

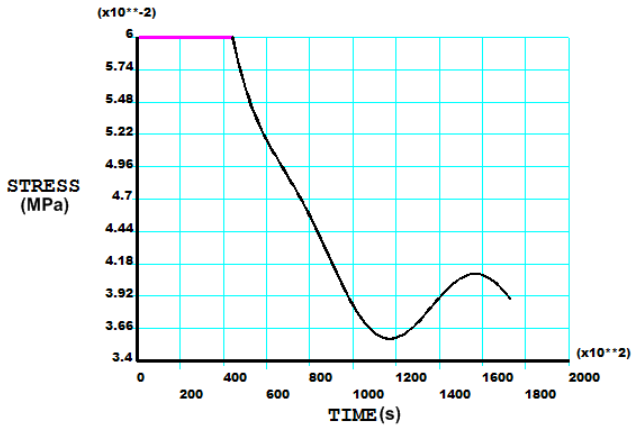

Figure 4.11: Stress results for node of maximum stress

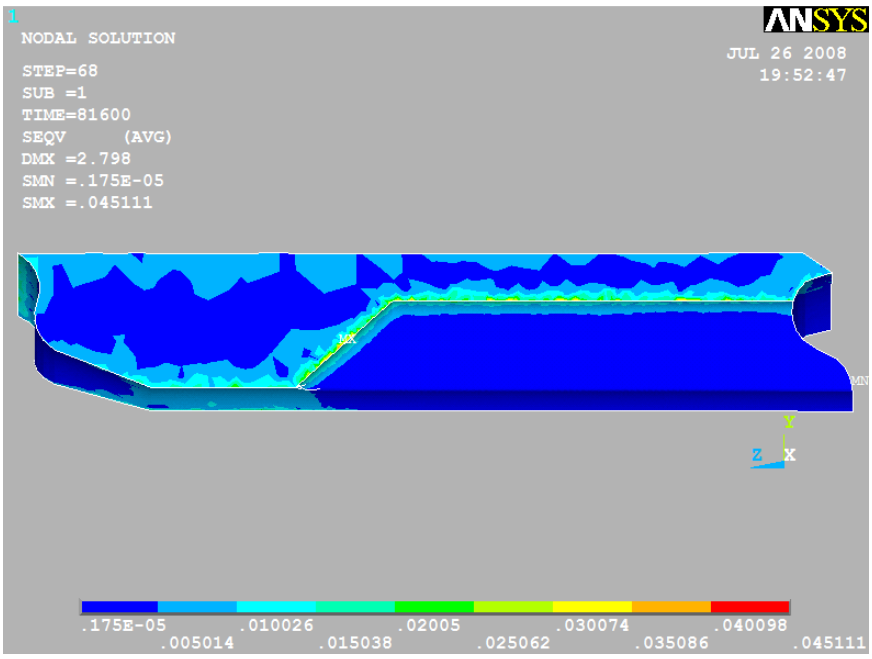

Figure 4.12: Stress field for an arbitrary time (MPa)

The results of structural analysis will later be used for cumulative damage analysis. Since stress levels of different locations in the propellant are different, critical locations must be determined for investigation of accumulated damage. In all the thermal stress analysis per-

formed in this study, the location of the maximum stress is found to be on the inner surface of transition section as shown in Figure 4.12.

CHAPTER 5

CUMULATIVE DAMAGE ANALYSIS

Cumulative damage analysis is performed to investigate the storage life of solid propellant grains. Accumulated damage is found through finite element analysis explained in previous chapters. The concept of cumulative damage and its application is explained in Chapter 2.

The value of accumulated damage ranges between 0 and 1, where the value 1 indicates failure. Therefore, the probability of failure can be defined as the probability of accumulated damage being higher than 1.

In this study, daily temperature changes are assumed to be cyclic and a methodology for predicting the amount of damage that is accumulated during a daily temperature cycle is developed. Each daily temperature cycle can be represented by a mean temperature value and amplitude. Therefore, daily accumulated damage is a function of grain geometry, material properties and mean and amplitude of the daily temperature cycle.

Twelve finite element analyses performed for each month's average daily cycle is used for assessing the accumulated damage in the grain. The temperature cycle (mean and amplitude), the stress cycle and daily damage at the location of highest stress are investigated. Detailed information on cumulative damage calculations is given in section 2.2.2.2. Table 5.1 and 5.2 summarize the data from the maximum stress region.

The mean temperature at an internal region of the grain is linearly related to the surface mean temperature. However, such a direct relation cannot be obtained for the amplitude of the temperature at an internal region. The amplitude at an inner region can only be related to both the mean and amplitude of the surface temperature. Figure 5.1 shows the mean temperature of the MSR versus mean surface temperature.

Table 5.1: Temperature cycles at the surface and maximum stress region (MSR)

	Mean of Surface Temperature	Amplitude of Surface Temperature	Mean of Temperature at MSR	Amplitude of Temperature at MSR
JAN	0.3	3.8	0.73	0.74
FEB	1.55	4.35	2.08	0.80
MAR	5.65	5.45	6.31	1.00
APR	11.2	6.1	12.02	1.04
MAY	15.8	6.4	16.66	1.09
JUN	19.5	6.9	20.42	1.18
JUL	22.65	7.25	23.53	1.33
AUG	22.7	7.3	23.58	1.34
SEP	18.55	7.25	19.52	1.24
OCT	13.4	6.6	14.28	1.13
NOV	7.65	5.25	8.35	0.90
DEC	2.7	3.6	3.14	0.66

Table 5.2: Stress cycle and accumulated damage at the maximum stress region (MSR)

	Mean of Stress at MSR	Amplitude of Stress at MSR	Accumulated Damage
JAN	0.03839	0.00259	7.193E-05
FEB	0.03738	0.00318	6.998E-05
MAR	0.03486	0.00381	7.099E-05
APR	0.03196	0.00329	6.737E-05
MAY	0.02964	0.00264	6.100E-05
JUN	0.02779	0.00231	5.410E-05
JUL	0.02622	0.00207	4.820E-05
AUG	0.02619	0.00208	4.820E-05
SEP	0.02827	0.00256	5.697E-05
OCT	0.03085	0.00314	6.585E-05
NOV	0.03378	0.00339	6.793E-05
DEC	0.03654	0.00263	6.547E-05

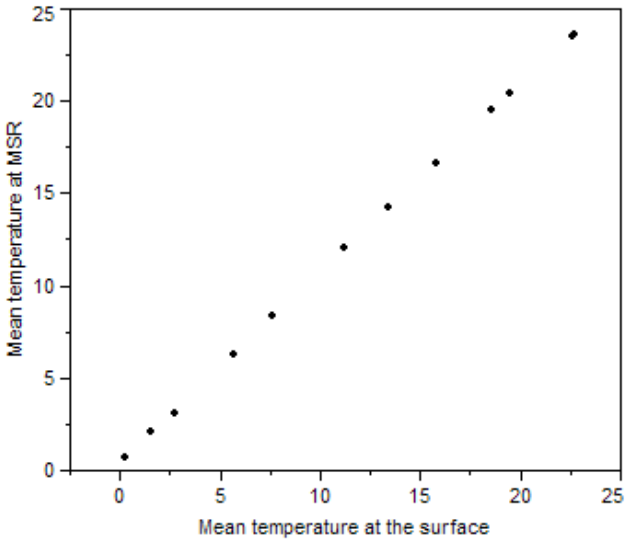

Figure 5.1: Mean temperature of MSR versus mean surface temperature

Mean of the stress value in the MSR can also be directly related to mean surface temperature where the amplitude of the surface can only be explained together with the amplitude of the surface temperature. Figure 5.2 shows the mean stress versus mean surface temperature.

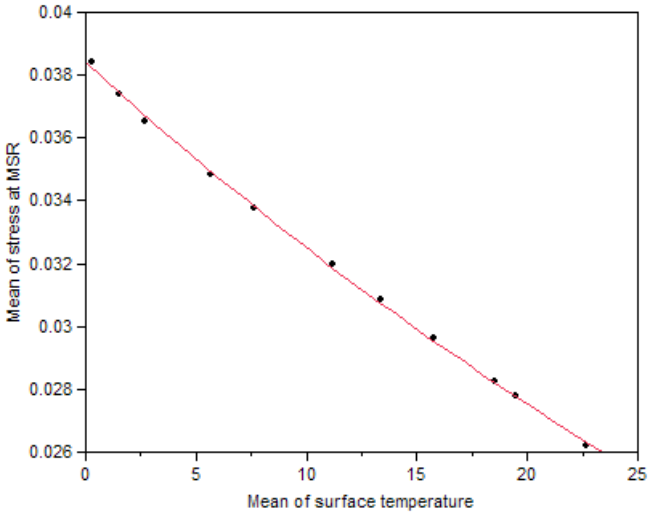

Figure 5.2: Mean stress versus mean surface temperature

In the process of evaluating the service life of the propellant grain and prediction of probability of failure, daily damage needs to be calculated many times for different mean and amplitudes of surface temperature. Considering the very long time that is required to obtain the daily damage through direct simulation methods, a surrogate model may alleviate the bur-

den and enable fast calculation of the daily damage. The previously stated relations support the possibility of such a surrogate model that can emulate the thermo-structural system to yield daily damage amount.

5.1 Daily damage model

Daily damage can also be modeled with several methods. The scarcity of the data makes it very difficult to construct a mathematical model for daily damage. Furthermore, for a surrogate model to prove its validity there has to be some cross validating data points not used to construct the model. Therefore, a careful selection of a surrogate model for daily damage is required.

As systems get more complex, more elaborate tools are needed to analyze them. These tools have to combine different disciplines to account functional interconnectivity between them [29]. Meta-modeling approaches allow building surrogate models that substitute complex models with approximate ones. Such meta-models are widely used in

- Parametric studies,
- Probabilistic analyses,
- Tradeoff studies.

Meta-modeling techniques can be grouped by the type of regression employed [29]. The polynomial based Response Surface Methodology can be categorized as the linear regression technique, while an example of a non-linear regression technique is Artificial Neural Networks.

5.1.1 Polynomial Based Response Surface

Response surfaces are models used to predict input - output relations of complex systems with rather simple polynomials. Response surfaces are generally constructed with second degree polynomials. However, it is possible to use third or higher order polynomials.

$$Y = \beta_0 + \beta_1 X_1 + \beta_2 X_2 + \beta_{12} X_1 X_2 + \beta_{11} X_1^2 + \beta_{22} X_2^2 + \ \ldots \tag{5.1}$$

, or in a more general form:

$$Y = \beta_0 + \sum_{i=1}^{k} \beta_i X_i + \sum_{i<j}^{k} \beta_{ij} X_i X_j + \sum_{i=1}^{k} \beta_{ii} X_i^2 + \ \ldots \tag{5.2}$$

Construction of the response surface models is realized by predicting the β coefficients by using the collected data. Prediction of the β coefficients is generally done by least squares regression.

After the polynomial coefficients are predicted, these coefficients are used to obtain predicted response values for each row of the data.

$$y_{predicted} = X.\beta_{predicted} \tag{5.3}$$

These values are used to calculate coefficient of determination (R^2) so that the prediction power of the constructed polynomial model can be assessed. This coefficient takes values between 0 and 1, and the closer it is to 1 the better the model is.

$$R^2 = 1 - \frac{SS_E}{SS_T} \tag{5.4}$$

Where SS_E and SS_T are defined as sum of squared errors and sum of squares respectively, defined as,

$$SS_E = \sum_{i=1}^{n} (y_i - y_{predicted_i})^2 \tag{5.5}$$

$$SS_T = \sum_{i=1}^{n} (y_i - \bar{y})^2 \tag{5.6}$$

Where $\bar{y}$ is the average of the response values in the data.

Although R^2 can be used to assess the goodness of fit, when the number of predicted coefficients increase, R^2 loses its accuracy. Therefore another coefficient called R^2_{adj} which is

independent of the number of coefficients predicted must be used. This coefficient also takes values between 0 and 1.

$$R^2_{adj} = 1 - \frac{SS_E/(n-k-1)}{SS_T/(n-1)} \tag{5.7}$$

Another visual method used to verify the constructed models is the cross validation. Sometimes it's impossible to detect by residual analysis or the data used to fit the model, if the constructed response surface model will work at points other than the data points used to construct it. For cross validation, data points other than the ones in the data used to fit the model are necessary. These data points are generally selected randomly within the region of interest. Actual response values are obtained for these random points the same way response columns of the data are obtained. Predicted response values for the same points are also obtained by using constructed response surface models. Then actual vs. predicted graphs are drawn for assessment of the response surface models. Data points lying on a 45 ° line is what should be seen for a valid response surface model. In other words, the more the collection of the points resembles a 45 ° line the better the model is.

The response surface model fitted to the daily damage is a second order polynomial. The goodness of fit seems to be sufficient for further studies. Two new analyses are performed through direct simulation in order to be used as cross validation points. These new data are not included in regression models; they are only used for validating the constructed surrogate models.

The summary of the fit is presented in Table 5.3. Figure 5.3 is the actual versus predicted plot for both the data used for fitting and cross validation points. The fitted surface can be seen in Figure 5.4.

Table 5.3: Summary of response surface fit

RSquare (R^2)	0.989094
RSquare Adj (R^2_{adj})	0.980005
Root Mean Square Error	1.21E-06
Mean of Response	6.23E-05
Observations	12

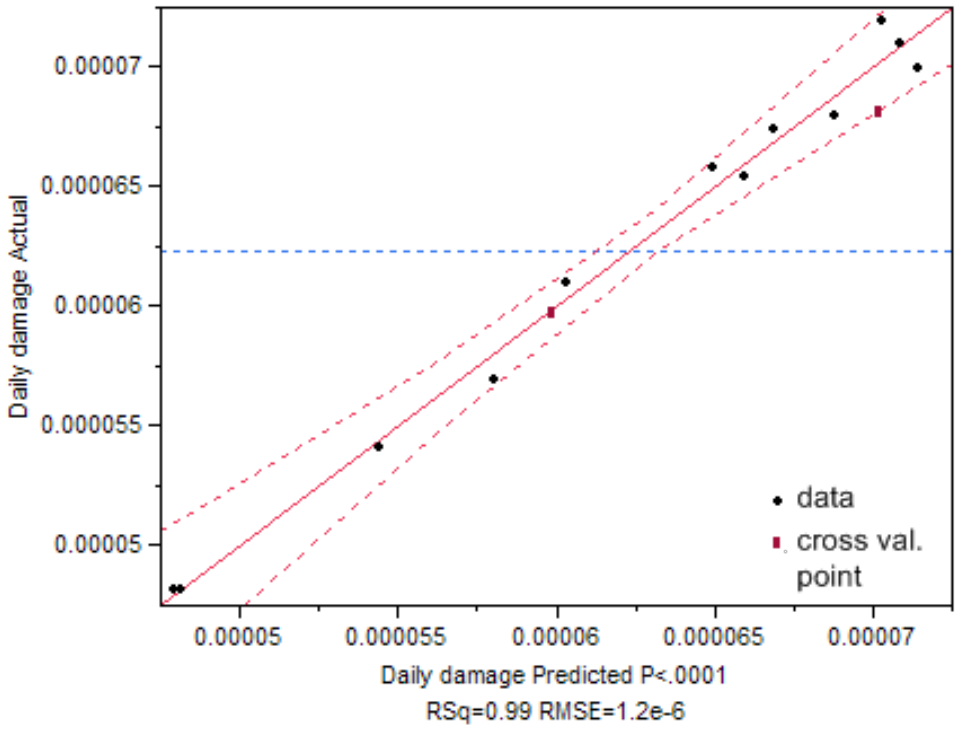

Figure 5.3: Actual versus predicted plot for response surface model

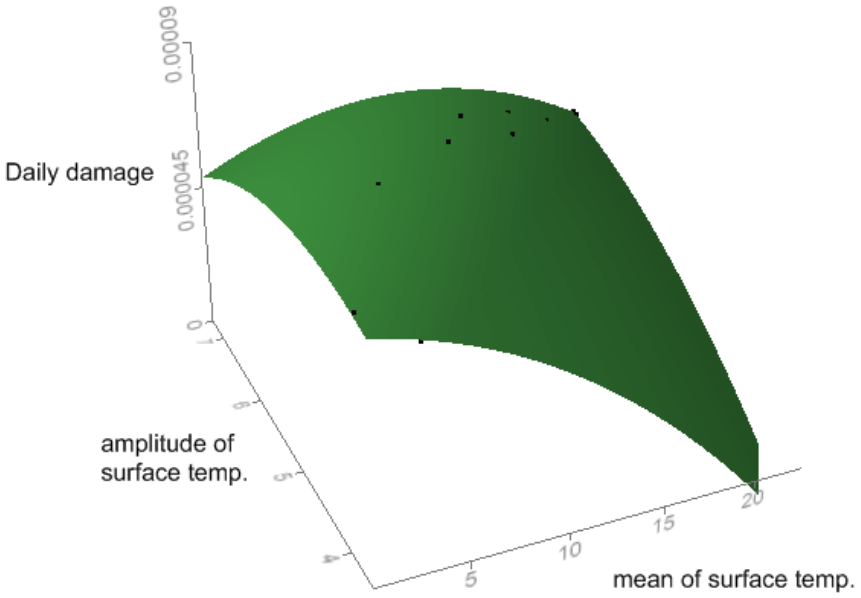

Figure 5.4: Response surface

5.1.2 Artificial Neural Networks

Neural network learning methods provide a robust approach to approximating real-valued, discrete-valued, and vector-valued target functions [30]. Inspired from the nature, artificial neural networks provide solutions for meta-modeling problems. Neurons and neural networks in living organisms are mimicked to form artificial neural networks. Figure 5.5 illustrates actual and artificial neurons.

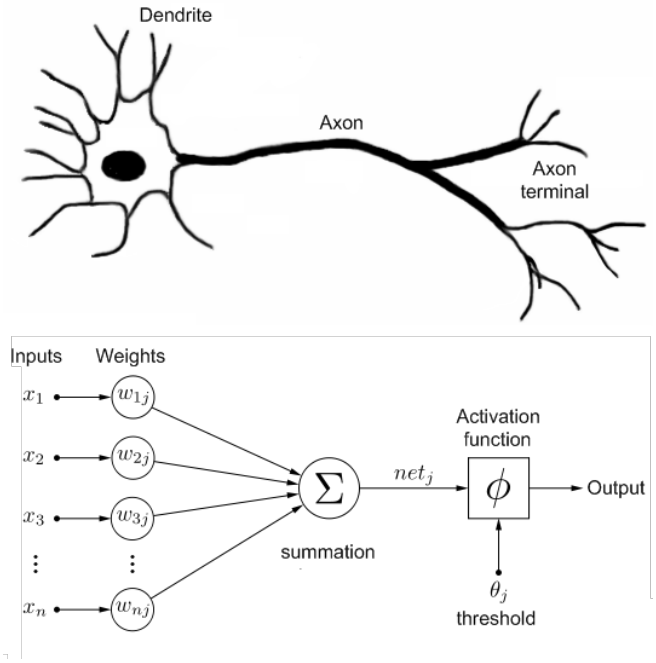

Figure 5.5: Natural and artificial neurons

Natural neurons receive electric signals from their dendrites, pass this signal along their axons, and transmit the signal to the neighboring neurons. Neurons, may manipulate these signals by amplifying or decreasing these signals. Artificial neurons are modeled to mimic this behavior. Artificial neurons consist of a unit that sums the inputs with certain weights, a threshold, an activation function, and an output. There are many activation functions found in the literature. One of the most commonly used activation functions for meta-modeling is the s-shaped sigmoid function (equation 5.8). Activation functions used in the neurons in this study are also sigmoid.

$$S(x) = \frac{1}{1 + \exp(-x)} \tag{5.8}$$

Neural networks are composed of layers of neurons which are connected with the neurons on the neighboring layer. It is possible to have a single hidden layer of neurons and an output layer as employed in this study (Figure 5.6).

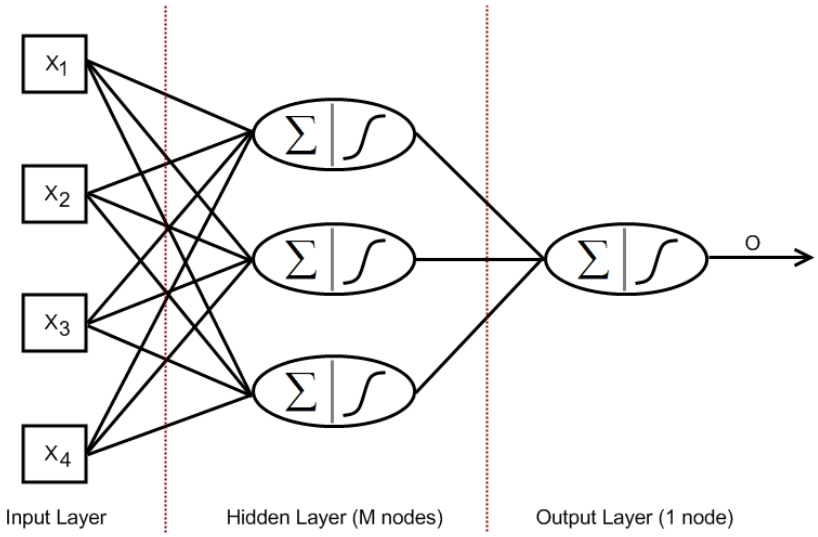

Figure 5.6: Generic two layer neural network

Non linear least-squares regression methods are used to determine the weighting factors in the neural network. Number of nodes to include in the hidden layer should be optimized with appropriate indicators. This can easily become a tricky task since rsquare almost always increases with increasing number of nodes while having high number of nodes brings the risk of overfitting.

Although they are very useful in modeling highly nonlinear systems, artificial neural networks carry the risk of overfitting. Overfitting can be defined as fitting a model that has too many parameters. Overfitting leads to arbitrariness in the fitted model parameters which can easily reduce or destroy the ability of the model to emulate the actual system or simulation.

Overfitting is not easy to detect without cross validation since the fitted model is very consistent when evaluated with the training data. Nevertheless, when used with new data, the

overfitted neural network produces arbitrary results.

In consequence of the overfitting problem, neural networks are generally fit with holdback samples to cross validate the model. These holdback samples are not used in the estimation process. The fitting data is usually called the training set, and the holdback samples are called the cross validation set. The two data points used as cross validating points are also held back in neural network studies to be used again for cross validating. Another tool used to avoid overfitting and improve the convergence is the overfit penalty or weight decay. This method puts a penalty on the size of the parameter estimates. Overfit penalty should also be optimized just like the number of nodes. Although increasing the overfit penalty reduces the risk of overfitting, it may cause lack of fit.

The necessity to optimize the number of nodes and overfit penalty makes the training of neural networks an iterative process. Therefore, indications for goodness of fit and overfitting are required. K-fold cross validation method can be used to obtain cross validation rsquare so that overfitting can also be inspected during the fitting process.

K-fold cross validation is suitable for use with small data sets. In this method data are partitioned randomly into k number of groups. K in this study is chosen to be 5 since the number of data is very few. After the data is grouped, the following procedure is followed.

- The model is fit to the complete data set
- Each of the k groups is then held back and the model is fit again to the rest of the data using the overall fit for starting values. Rsquare is calculated using the holdback group.
- After iterating all the groups, the calculated cross validation rsquare (CVRsquare) values are averaged to yield the overall CVRsquare.

Although k-fold cross validation is computationally very intensive when compared to a simple holdback cross validation, it is more reliable for small data sets.

The steps followed to fit the neural network[1] for the daily damage are summarized in Table 5.4. The actual versus predicted plot including the holdback cross validating points is illustrated in Figure 5.7. The resulting surface can be seen in Figure 5.8.

[1] In this study all the neural network trainings are carried out with the statistical software package SAS JMP.

Table 5.4: Neural network fit history

Step	Nodes	Overfit Penalty	RSquare	CV RSquare
1	3	0.001	0.99709	0.88228
2	4	0.001	0.99864	0.89209
3	5	0.001	0.9969	0.90192
4	6	0.001	0.99772	0.90998
5	7	0.001	0.9978	0.90816
6	6	0.001	0.99774	0.90996
7	6	0.01	0.99135	0.92906
8	6	0.02	0.9885	0.92632
9	6	0.01	0.99134	0.92954

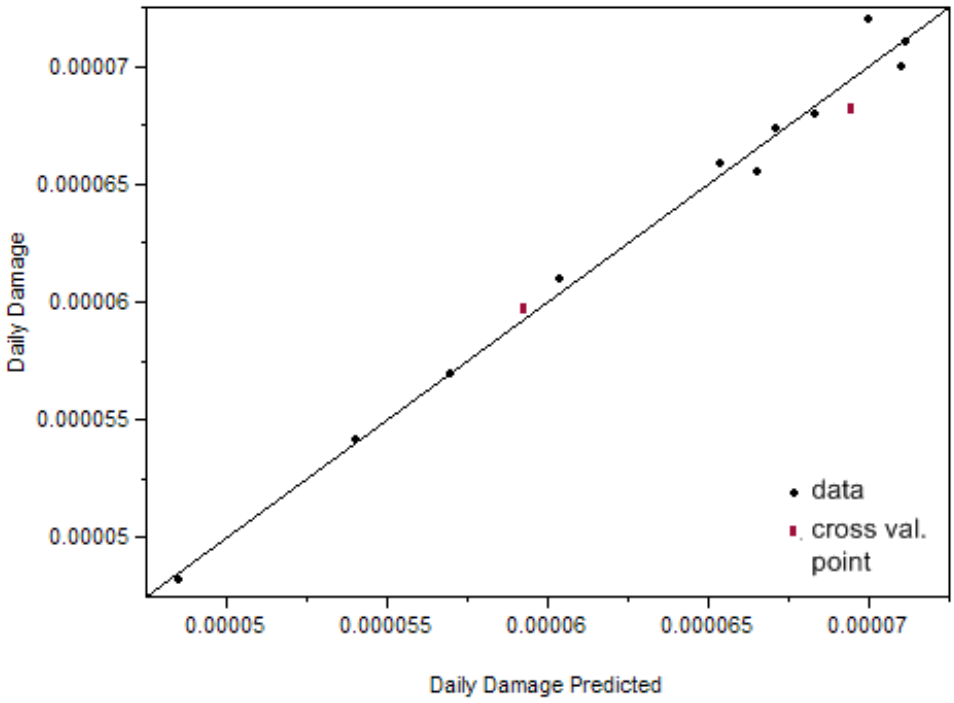

Figure 5.7: Actual versus predicted plot for neural network model

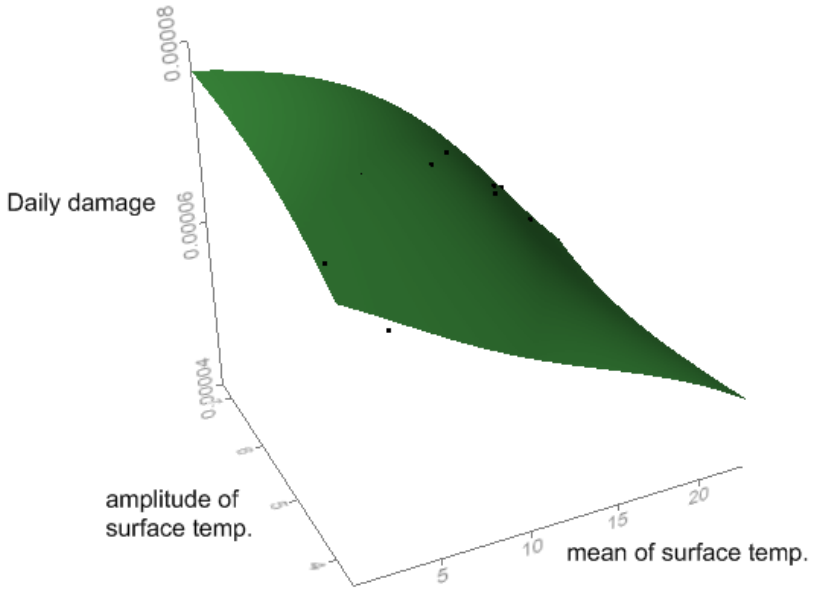

Figure 5.8: Neural network surface

When the response surface and neural network models constructed for daily damage are examined, neural network model is slightly better and will be used for further studies. However, response surface model can also be used when a simpler meta-model is required. The major metric used for comparison of the two meta models is the coefficient of determination.

5.2 Daily temperature cycle

Daily temperature cycle can be represented with its mean and amplitude. In the analyses performed in previous sections, a fixed cycle for each month was chosen. However, when daily temperature cycles within a month are examined, there obviously is randomness in both the mean and amplitude of the daily cycle.

Average daily temperatures of Ankara[2] from 1995 to 2008 are statistically examined. The mean daily temperatures for each month can be assumed to be distributed normally (Appendix B.1). Daily temperature amplitude is taken according to Table 4.1. The amplitude is also assumed to be normally distributed with a coefficient of variation of 10%. Table 5.5 gives

[2] Average daily temperatures of Ankara are taken from the Average Daily Temperature Archive of the University of Dayton

the means and standard deviations of daily temperature means and amplitudes. Accumulated damage within a year will be calculated according to these values.

Table 5.5: Daily temperature cycles

Month	Mean of Mean temp	Standard dev. of Mean temp	Mean of Amplitude	Standard dev. of Amplitude
JAN	-1.333	5.031	3.800	0.380
FEB	0.159	4.363	4.350	0.435
MAR	4.570	4.188	5.450	0.545
APR	9.166	3.912	6.100	0.610
MAY	14.786	3.279	6.400	0.640
JUN	18.570	3.103	6.900	0.690
JUL	22.319	3.001	7.250	0.725
AUG	22.333	3.014	7.300	0.730
SEP	16.771	3.077	7.250	0.725
OCT	11.355	3.856	6.600	0.660
NOV	4.731	3.938	5.250	0.525
DEC	0.818	4.153	3.600	0.360

5.3 Accumulated damage

In order to obtain monthly damage amount for each month, the probability distribution of daily damage for each month is found. Monte Carlo simulations with 100,000 samples are used with the artificial neural network model to obtain the daily damage distributions of each month. The methodology used in Monte Carlo simulations is illustrated in Figure 5.9. The probability distributions of daily damages are found to conform to normal distribution properties (Appendix B.2). Therefore, monthly damage amounts are found through multiplication of these distributions with the number of days in the month. Table 5.6 gives the statistical properties of the daily damage amounts for each month. The monthly damages are found as follows:

$$\mu_m = n_{days}\mu_d \tag{5.9}$$

$$\sigma_m = \sqrt{n_{days}\sigma_d} \tag{5.10}$$

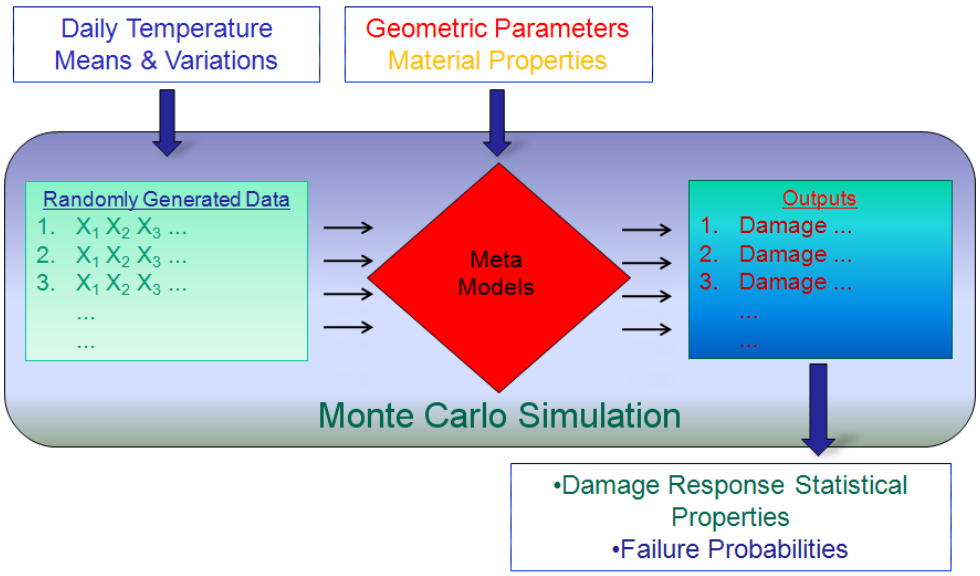

Figure 5.9: Monte Carlo simulation

Table 5.6: Daily damage amounts

month	Mean of daily damage	Standard dev. Of daily damage
JAN	7.11E-05	4.80E-06
FEB	7.19E-05	4.23E-06
MAR	7.17E-05	4.48E-06
APR	6.89E-05	5.26E-06
MAY	6.17E-05	5.98E-06
JUN	5.60E-05	6.28E-06
JUL	4.98E-05	5.75E-06
AUG	4.98E-05	5.77E-06
SEP	6.03E-05	6.09E-06
OCT	6.75E-05	5.86E-06
NOV	7.09E-05	4.36E-06
DEC	6.84E-05	4.37E-06

Where μ_m and σ_m are mean and standard deviation of monthly damage, μ_d and σ_d are mean and standard deviation of daily damage of the corresponding month, and n_{days} is the number of days the month comprises.

Once the amount of damage that accumulates during each month is found, it is finally possible to calculate the damage that accumulates during a one year period using the equations below:

$$\mu_y = \sum_{m=1}^{12} \mu_m \tag{5.11}$$

$$\sigma_y = \sqrt{\sum_{m=1}^{12} \sigma_m^2} \tag{5.12}$$

Where μ_y and σ_y are the mean and standard deviation of accumulated damage within a year.

When the operations in equations 5.9 - 5.12 are carried out for the case investigated in this study, the mean of yearly damage is found as 0.0235 and the standard deviation of the yearly damage is found as 0.000103.

5.4 Probability of failure

When damage accumulated in the propellant grain is statistically characterized, it is possible to determine the probability of failure under appropriately defined failure criteria. A failure criterion that relies on the accumulated damage can be defined such that if accumulated damage passes a predefined barrier, failure would occur.

Under ideal circumstances, the structural failure of the grain would occur when the accumulated damage reaches the value of one. This is not the case when only storage loads are considered. It is not an overstatement to say that solid propellant grain accumulates most of the damage during pressurization at ignition and burnout, and the cool down period following the curing process. Considering these facts, the barrier for the accumulated damage during storage shall be chosen carefully so that the propellant would still be operable after the storage period.

Furthermore, the damage accumulated during cool down and operation is also statistically variable. Therefore, it is not meaningful to set constant barriers for the accumulated dam-

age. The barrier should also be statistically variable. Under guidance of past experience, for demonstration purposes the accumulated damage barrier is assumed to be distributed normally with a mean of 0.5 and standard deviation of 0.1.

Under these circumstances failure occurs when accumulated damage passes the failure barrier which also is statistically variable. For probability of failure to be formulated, the accumulated damage needs to be parameterized depending on time. Hence, in a yearly time scale the following relation can be postulated.

$$\mu_{yt}(t) = \mu_y t \tag{5.13}$$

$$\sigma_{yt}(t) = \sqrt{t}\sigma_y \tag{5.14}$$

Where μ_{yt} and σ_{yt} are time dependent mean and standard deviation of accumulated damage, and t is time in years.

The probability of failure can now be defined as

$$F(t) = P(yt(t) \geq barrier) \tag{5.15}$$

Where yt is the accumulated damage as postulated in equation 5.13 and 5.14. A limitstate function can be defined such that equation 5.15 is transformed into

$$F(T) = P(LS(t) \geq 0) \tag{5.16}$$

Where

$$LS(t) = yt(t) - barrier \tag{5.17}$$

Therefore $LS(t)$ can further be statistically characterized as follows

$$\mu_{LS}(t) = \mu_{yt}(t) - \mu_{barrier} \tag{5.18}$$

$$\sigma_{LS}(t) = \sqrt{\sigma_{yt}(t)^2 + \sigma^2_{barrier}} \tag{5.19}$$

It is now possible to calculate probability of failure using the cumulative distribution function of the limitstate function's distribution which is normal since it is a combination of two normal distributions. The probability of failure is plotted versus time in Figure 5.10.

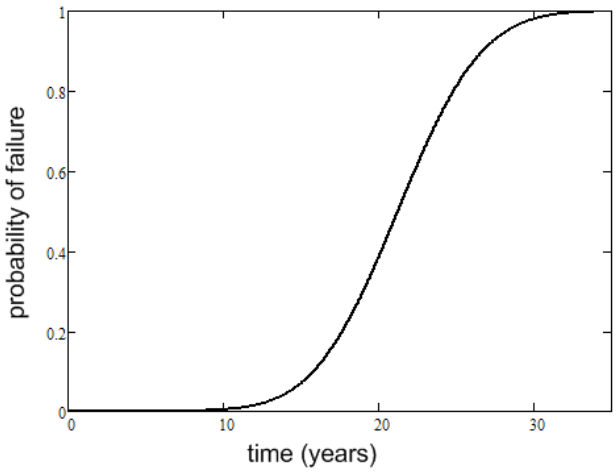

Figure 5.10: Probability of failure

CHAPTER 6

DISCUSSION

Design of solid propellant grains is a complicated multidisciplinary task. Design tools used for structural analysis, burnback analysis and others shall be in harmony. Designers should have the ability to perform multidisciplinary optimization and trade-off studies for a given design process without the need to construct the propellant geometry on many different platforms.

Possession of a parametric propellant grain design tool alleviates the burden in many different aspects. First of all it brings the ability to react swiftly to the design changes when they occur frequently especially in early design phases. If the coordination of other design tools with the parametric grain designer, which actually is an automatic geometry generator, is provided, then it is possible make early judgments on any proposed design and have more insight of the design at the stage it is proposed. Moreover, being able to have more information on the design in early stages allows the designers to optimize the design faster and minimize the engineering changes made throughout the design process. Therefore, having the right tools work in unison saves both time and money.

The parametric design tool developed in this study, namely GrainPar, provides solutions for many problems mentioned above. It can be depicted as a flexible solid propellant grain design platform which is able to talk with other design tools and provide ease of use for the designers throughout the iterative design process.

Necessity of such a tool is obvious. Nevertheless, it is not the only means for achieving a reliable and optimized design. Being focused on certain aspects of the product under design while ignoring others may lead to frustration in later design phases where engineering changes are much more difficult and costly. Therefore, for a complete assessment of the design, all aspects of the design should be taken into consideration.

Reliability based design methodologies provide many possibilities for accomplishing detailed evaluations of designs. Furthermore, reliability based design optimization may become the most appropriate tool for multidisciplinary design optimization problem for some cases. However, the danger of ignoring certain aspects of the design still exists. All the important failure modes of the system should be determined and included in the analysis with consistent failure criteria. Reliability based design methods are useful only if all governing failure modes of the system are included.

Storage reliability of solid propellant grains is one of the most commonly disregarded fields in solid propellant design. Due to long storage periods, lower loads during storage and relatively less known behavior under these long term loads, storage reliability prediction is commonly left out of the design process. However, as service life of defense systems are becoming more and more important, service life studies and storage reliability predictions are attracting interest. Furthermore, being able to predict service life in early design phases allows optimizing the design and logistic support procedures for required service life.

This study shows that, with the engineering tools used in design of solid propellant grains, it is also possible to make predictions on service life or storage reliability of the propellant grains.

Cumulative damage methods are very useful for prediction of service life of solid propellants. Cumulative damage analysis can easily be applied with finite element analysis allowing the use of cumulative damage concepts with readily available tools.

Figure 6.1 is a plot of average daily damage and mean temperature for each month. The relation between daily damage and temperature is more complicated than the relation between stress levels and temperature.

As shown in Figure 5.2, stress levels are directly related to temperature levels. Stress levels rise as the temperature decreases. Contrary to intuition, the cumulative damage analyses performed in this study showed that such a direct relation does not exist for temperature and damage as seen in Figure 6.1. In other words, due to temperature dependency of the material higher stress levels don't always mean higher damage. Similar findings exist in Heller's studies [19].

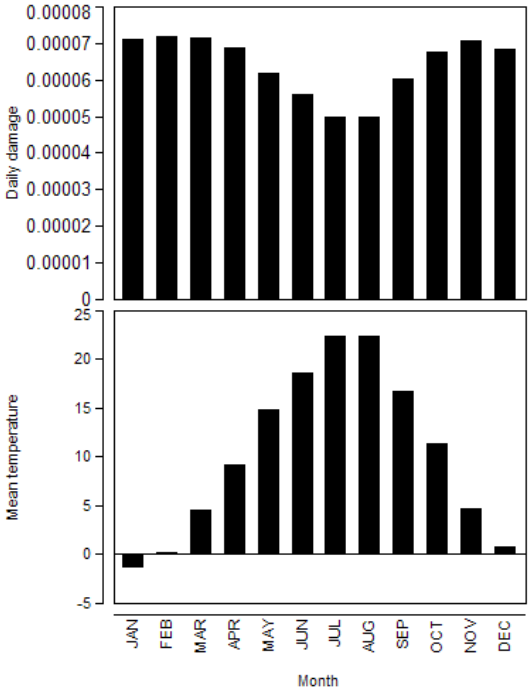

Figure 6.1: Average daily damage and mean temperatures

It is shown that damage is significantly affected by the temperature shift properties of the propellant. Therefore, even though lower stresses occur at higher temperatures, due to domination of the shift factor in the damage relation (equation 2.62) the damage does not decrease as swiftly as the stress with rising temperature. There may even be cases where the amount of damage actually increases with rising temperature.

These findings imply that if protected storage is planned, storage conditions should be selected correctly to provide the right environment for the propellant to accumulate minimum damage. Propellants are generally protected from cold. However, as mentioned here, for some propellants, colder environments may be more protective. Careful characterization studies and cumulative damage analyses should be carried out to determine the most protective environment.

Since the emphasis is on thermal stresses in this study, region of highest stress doesn't differ from one analysis to another. The region of maximum stress is shown in Figure 6.2. These findings conform with the studies of Faulner and Tod [35]. However, if other loads are more effective, the region of maximum stress may be different for every analysis. In that case cumulative damage analyses should be carried out for more than one critical region and accu-

mulated damage should be monitored for each and every one of these critical regions. There may also be cases where more than one failure criteria is used such as maximum principal strain criterion and effective stress criterion. Each of the criteria may result with different critical regions. Therefore, monitoring of the accumulated damage in all of these regions is required in such a case too.

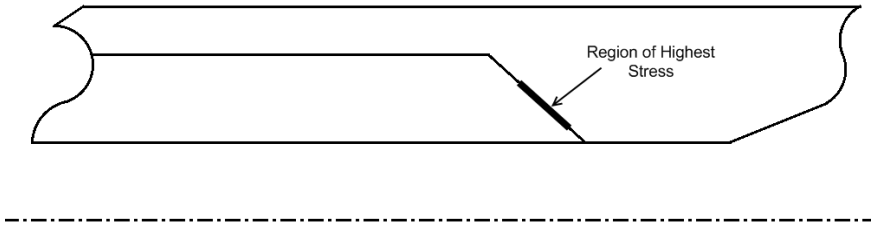

Figure 6.2: Region of highest stress

There are no strict structural failure criteria established for solid propellants. There are many different recommendations in the literature on how to make structural assessments of solid propellants. Under guidance of these past experience and recommendations, exploration of structural failure criteria should be included in the material characterization studies. Appropriate failure criteria for the postulated failure modes should be determined in this stage. This would improve confidence in cumulative damage analyses and allow more accurate predictions of service life.

For more accurate methods for service life prediction to be developed, further experimental studies should be carried out. First of all, measurement of storage strains and stresses should be made in order to refine material models and finite element models. After conducting such experiments, Margetson and Wong [22] point out the benefits of such a study.

There are also studies in the literature explaining the failure of solid propellants with more extensive fracture mechanics. Failures in solid propellants generally occur by propagation of cracks. Therefore, propagation of cracks is actually what we call damage accumulation.

Solid propellants are particulate composite materials, containing hard particles embedded in a rubbery matrix. Or in other words they consist of a lightly crosslinked polymer, highly filled with relatively coarse solid particles. On the microscopic scale, a highly filled propellant can be considered as non-homogeneous. Ingredients of a typical composite solid propellant

are Ammonium perchlorate crystal particles of sizes 20μ[1] and 200μ functioning as oxidizer, aluminum powder particles of diameter 30μ functioning as the fuel, and polybutadiene rubber functioning as the matrix/binder and also as fuel. [32]

When the material is strained, damage in the form of microvoids in the binder or debonding at the matrix/particle interface takes place. As the applied strain in the material is increased the damage growth takes place as successive nucleation and coalescence of the microvoids or as tears. These processes of damage initiation and propagation are time dependent and they are mainly responsible for the time sensitivity of the non-linear stress-strain behavior of solid propellants. Material's mechanical response is strongly influenced by the loading rate, temperature and material microstructure. [34]

As in many studies carried out by Liu[31, 32, 33], crack propagation in stored solid propellants can be monitored by non-destructive testing techniques.

A test and experimentation scheme that includes non-destructive testing of stored propellants is a very comprehensive study which may be described as life monitoring. Such a study would require testing of stored propellants which may be either produced for this particular study or be already stored for service. Therefore, if production of a series of propellants is already planned, non-destructive monitoring of these propellants with predetermined intervals is not as costly as one may think. The tested articles may be returned back to service since the monitoring techniques are non-destructive.

Outputs of such a life monitoring program may allow construction of more accurate relations between crack sizes and damage. Furthermore, it would provide invaluable information for life extension studies.

Emphasis on cumulative damage parameters during material characterization also plays an important role cumulative damage analysis. Cumulative damage parameters should be determined keeping in mind the types of loads the propellant is exposed when stored. Reduced life curves should include extreme values to allow reliable predictions of service life.

Service life prediction is an extensive study which should be planned ahead. Its interaction with other constitutive design exercises should always be kept in mint. Otherwise, it would not be possible to make reliable service life or storage reliability predictions.

[1] $1\mu = 10^{-6}$ meter

CHAPTER 7

CONCLUSION AND FUTURE WORK

In the course of this thesis study, development of a solid propellant storage life prediction methodology was aimed. In order to accomplish this goal, a parametric grain geometry generator called GrainPar was created. Thermal stresses that occur under storage conditions are calculated by coupled thermal and structural finite analyses carried out in ANSYS. These stress values are used for the estimation of the accumulating damage in the propellant.

This study and its findings support that, it is possible to make numerical predictions for the storage life of solid propellants even in the early design phases. As more and more reliability of systems gains significance practical methods for reliability prediction become inevitable.

Ability to make reliable storage life predictions allows the optimization of the design to provide the required service life of the propellant. Furthermore, storage reliability predictions pool into the general reliability analyses to enable comprehensive reliability prediction studies.

Although the structural analyses are carried out for only one failure criteria, the methodology explained in this thesis can be applied with any structural failure criteria combination for assessment of different propellant failure types. As discussed in previous chapters, appropriate failure criteria should carefully be chosen for determined failure modes.

Material properties play an important role in both the finite element analyses carried out for the storage conditions and the cumulative damage analysis. Hence, requirements of these analyses should be taken into account during the material characterization studies. Distinctive characterization tests performed particularly for storage life prediction studies may sometimes be required.

The cumulative damage analyses carried out in this thesis also points out the need for particular attention at the adjustment of the correct protective environment for the propellant. By instinct, propellants are generally protected from cold since stress levels increase with decreasing temperature. However, when materials time-temperature shift properties dominate over the stress levels, higher damage accumulation may occur at higher temperatures even though the stress levels are lower. Therefore, when storage of solid propellants under controlled environments is planned, cumulative damage analyses should be carried out the determine the storage temperatures required for minimum damage accumulation.

Damage analysis that only comprises the storage loads is not sufficient for the prediction of storage life. The propellant also accumulates damage during the cool down and operation phases. These damages should also be evaluated for a complete storage life prediction study. The storage life should be determined such that the propellant should operate reliably after storage.

Finally, the methodology demonstrated in this study can be applied for a comprehensive storage life study. The case study examined in this study only takes the variations in the temperatures into account. With the necessary computational infrastructure provided, variations in the geometric features and material properties of the propellant can be included in the study to improve understanding of the factors affecting the storage life of solid propellants.

7.1 Recommendations for future work

The methodology presented in this thesis provides a basis for storage life predictions that can further be advanced with additional studies. These studies can be listed as follows.

- For more precise calculation of storage stresses, non-linear viscoelasticity has to be evaluated as a material model option. Material characterization tests should be carried out in order to evaluate the non-linear behavior of the propellant material. Consistent finite element methods should be developed to incorporate these non-linear material models into the structural analyses.

- Experimental studies should be carried out in order to obtain better relation between the crack propagation and damage or structural failure. Extensive non destructive testing of

stored propellants should be carried out to allow verification and refinement of storage life prediction methods.

- Elaborate failure qualification tests shall be performed for better understanding of structural failure criteria. Special attention is required for determining the best criteria for case debonding and bore cracking. Strain in viscoelastic materials, is as important as the stress. Failure criteria involving strain should be included in the cumulative damage analyses.

- For exploration of other factors that affect the damage accumulation more variables should be included in the studies. Material properties and geometric features of the propellants should be evaluated for their affects on the storage life. For efficient screening of these variables and better sensitivity analysis, design of experiment techniques should be applied in determination of the analyses to be run. The use of design of experiments techniques would also improve accuracy of the meta-models.

- Other loads that the solid propellant is exposed during its life cycle such as the transportation vibrations should be included in cumulative damage analysis for more precise life predictions.

- Application of these techniques at preliminary design phases of a rocket motor design project would allow reliability based design methodologies to be utilized with more confidence. Furthermore, it would allow the candidate designs to be evaluated taking their service lives into consideration.

REFERENCES

[1] Advisory Group for Aerospace Research & Development (AGARD-NATO): Structural Assessment of Solid Propellant Grains, AGARD-AR-350, 1997.

[2] Roys GP: User's manual for solid propulsion optimization code (SPOC) Volume II - User's Guide, ADA108225, 1981.

[3] Gökay Püskülcü: Analysis of 3-D Grain Burnback of Solid Propellant Rocket Motors and Verification With Rocket Motor Tests. MS Thesis, The Graduate School of Natural and Applied Sciences of the Middle East Technical University, 2004.

[4] MA Meyers, KK Chawla: Mechanical Behavior of Materials. Prentice Hall, 1999, pp. 98-103.

[5] Christensen RM: Restrictions upon viscoelastic relaxation functions and complex moduli. Trans. Soc. Rheol. 16, pp. 603-614, 1972.

[6] Roderic S. Lakes: Viscoelastic Solids. CRC Press, 1998, pp. 20-23.

[7] Tobolsky AV, Eyring H: Mechanical Properties of Polymeric Materials, J. Chem. Phys. 11, pp. 125-134, 1943

[8] Leaderman H: Elastic and Creep Properties of Filamentous Materials and Other High Polymers. The Textile Foundation. Washington DC, USA, 1943

[9] Ferry JD: Mechanical Properties of Substances of High Molecular Weight. VI. Dispersion in Concentrated Polymer Solutions and its Dependence on Temperature and Concentration, J. Am Chem. Soc. 72, pp. 3746-3752, 1950

[10] Brinson LC: Time-Temperature Response of Multi-Phase Viscoelastic Solids Through Numeric Analysis, PhD thesis, Caltech, Pasadena CA USA, 1990.

[11] Tameroğlu Sacit: Elastisite Teorisi. İstanbul Teknik Üniversitesi İnşaat Fakültesi Matbaası, pp. 98-100, 1991.

[12] E.J.S Duncan, Margetson J: A Nonlinear Viscoelastic Theory for Solid Rocket Propellants Based on a Cumulative Damage Approach. Propellants, Explosives, Pyrotechnics 23, pp. 94-104, 1998.

[13] Findley WN, Lai JS, Onaran K: Creep and Relaxation of Nonlinear Viscoelastic Materials, 2nd ed., Dover, New York, 1989.

[14] M. A. Miner: Cumulative Damage in Fatigue, J. Appl. Mech. 12, pp. 159-164 (1945)

[15] Svob GJ, Bills KW Jr: Structural Design Nomograph for thermal cycling of tactical rocket propellants. NWC Tech Tech Memo 3365, 1977.

[16] Bills KW Jr, Wiegand JH: The application of an Integrated Structural analysis to the Prediction of Reliability. Annals of Reliability and Maintainability, 1970, pp. 514-526

[17] Heller RA, Kamat MP, Singh MP: Probability of Solid-Propellant Motor Failure Due to Environmental Temperatures. Journal of Spacecraft and Rockets, Vol.16 No.3, 1978, pp. 140-146.

[18] Heller RA, Singh MP: Thermal Storage Life of Solid-Propellant Motors. Journal of Spacecraft and Rockets, Vol.20 No.2, 1983, pp. 144-149.

[19] Heller RA, Singh MP, Zibdeh H: Environmental Effects on Cumulative Damage in Rocket Motors. Journal of Spacecraft and Rockets, Vol.22 No.2, 1985, pp. 149-155.

[20] Thangjitham S, Heller RA: Stress Response of Rocket Motors to Environmental Thermal Loads. Journal of Spacecraft and Rockets, Vol.23 No.5, 1986, pp. 519-526.

[21] Zibdeh H, Heller RA: Rocket Motor Service Life Based on the First-Passage Method. Journal of Spacecraft and Rockets, Vol.26 No.4, 1989, pp. 279-284.

[22] Margetson J, Wong FC: Service Life Prediction of Solid Rocket Propellant Motors Stored in a Random Thermal Environment. AGARD Conference Proceedings 586, Service Life of Solid Propellant Systems, Athens, Greece, 1996.

[23] Chen JT, Leu SY: Finite Element Analysis, Design and Experiment on Solid Propellant Motors With a Stress Reliever. Finite Elements in Analysis and Design, 29, 1998, pp. 75-86.

[24] Chyuan SW: A Study of Loading History Effect for Thermoviscoelastic Solid Propellant grains. Computers and Structures, 77, 2000, pp. 735-745.

[25] Akpan UO, Wong FC: The Role of Probabilistic Sensitivity Analysis in Assessing the Service Life of Solid Rocket Motors. AIAA 2002-1714. 43rd AIAA/ASME/ASCE/AHS/ASC Structures, Structural Dynamics, and Materials Conference, Denver, Colorado, 2002.

[26] Si H, Gaertner K: Meshing Piecewise Linear Complexes by Constrained Delaunay Tetrahedralizations. Proceedings of the 14th International Meshing Roundtable, pp. 147-163, September 2005.

[27] Si H: On Refinement of Constrained Delaunay Tetrahedralizations. Proceedings of the 15th International Meshing Roundtable, September 2006.

[28] Si H: TetGen A Quality Tetrahedral Mesh Generator and Three-Dimensional Delaunay Triangulator Version 1.4 User's Manual, 2006.

[29] Kuran B: Reliability Based Design Optimization of a solid Rocket Motor Using Surrogate Models. 43rd AIAA/ASME/SAE/ASEE Joint Propulsion Conference and Exhibit, Cincinnati, OH, July 8-11, 2007. AIAA-2007-5825

[30] Tom M. Mitchell: Machine Learning. McGraw-Hill, 1997. pp 81-82.

[31] Liu CT: Evaluation of damage fields near crack tips in a composite solid propellant. Journal of Spacecraft and Rockets. Vol.28 No.1, 1991, pp. 64-70.

[32] Baron DT, Miller TC, Liu CT: Subcritical Crack Growth in Composite Solid Propellant. Air Force Research Laboratory Technical Paper. CA USA. 1998.

[33] Liu CT: Crack growth behavior in a solid propellant. Engineering Fracture Mechanics, 56:1 pp. 127-135, 1997.

[34] Gdotos EE, Papakaliatakis: Study of crack growth in solid propellants. Fatigue Fract Engng Mater Strruct 24, pp. 637-642. 2001.

[35] Faulkner GS, Tod D: Service life prediction methodologies aspects of the TTCP KTA-14 UK programme. AGARD Conference Proceedings 586, Service Life of Solid Propellant Systems, Athens, Greece, 1996.

APPENDIX A

MATERIAL MODEL

The linear viscoelastic material model used in the analyses is presented in this appendix. The master curve obtained from material characterization tests is shown in Figure A.1. The prony series fitted to this master curve, together with other material properties are given in Table A.1.

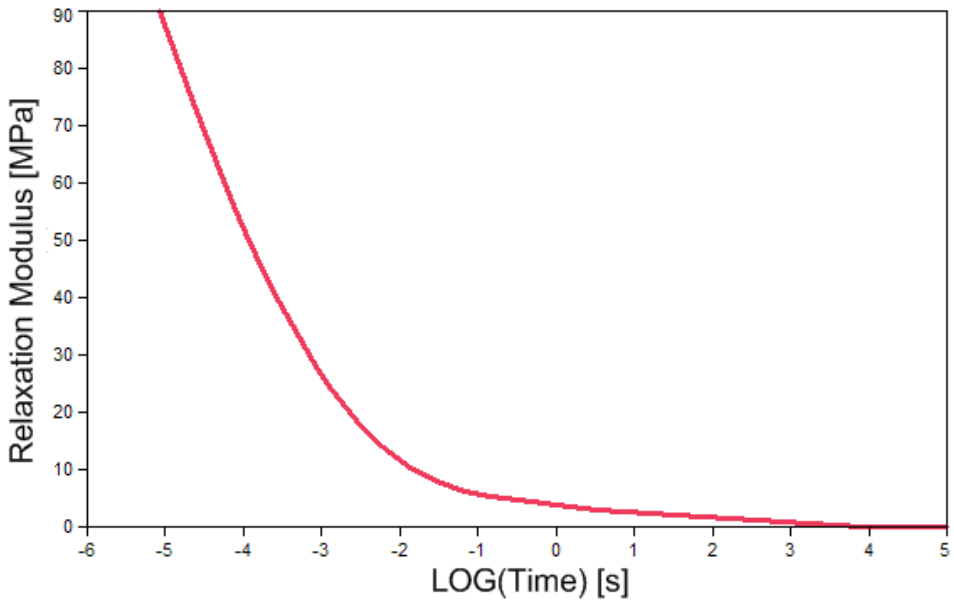

Figure A.1: Master curve

Figure A.2, illustrates the time temperature shifting. Master curve is drawn for 25°C. To obtain the relaxation curves of other temperatures, the shift factor for that temperature has to be found. The required parameters T_{ref}, C_1, and C_2 are given in Table A.1.

Table A.1: Material properties

Density:	1800 kg/m^3	
Poisson's Ratio:	0.499	
Coefficient of Thermal Expansion:	8.50E-05	
Prony Series:		
	E_i (MPa)	τ_i (s)
	50	3.20E-05
	30	0.0007
	12	0.012
	2	1.2
	1	170
	0.8	2700
Shift parameters:		
	Tref:	25°C
	C1:	-8.8
	C2:	250

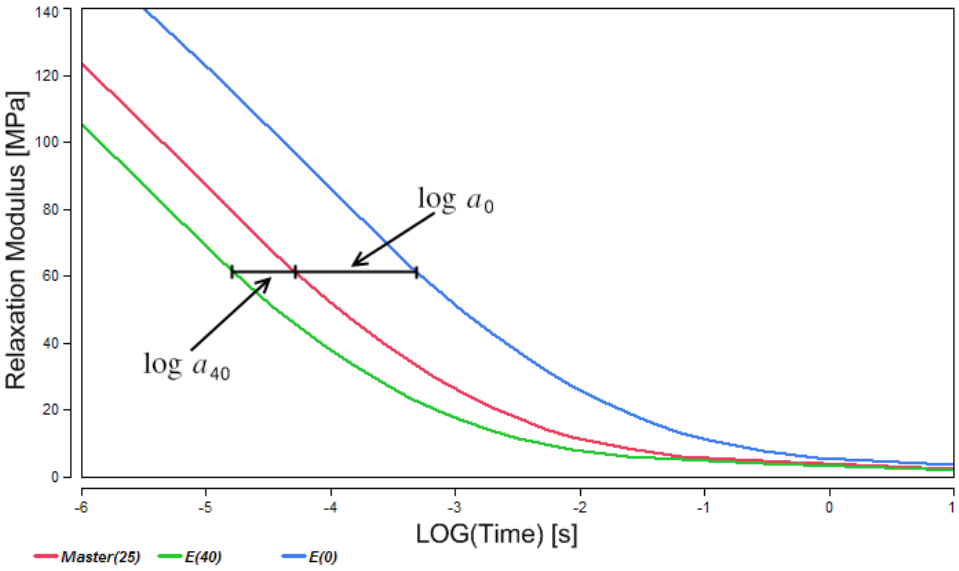

Figure A.2: Illustration of time-temperature shifting

In Figure A.2, other than the master curve, two relaxation curves that belong to different temperatures (40°C and 0°C) are drawn by shifting the master curve horizontally. Note that horizontal shifting of the master curve is only possible if the time scale is logarithmic. The amount of shift is defined by the shift factor calculated for the related temperature. The calculation of these shift factors are shown in the following equations.

$$\log a_{40} = \frac{C_1\left(40 - T_{ref}\right)}{C_2 + \left(40 - T_{ref}\right)} = -0.498 \tag{A.1}$$

$$\log a_0 = \frac{C_1\left(0 - T_{ref}\right)}{C_2 + \left(0 - T_{ref}\right)} = 0.978 \tag{A.2}$$

As seen in Figure A.2, the relaxation curves of temperatures higher than the reference temperature are on the left hand side of the master curve, whereas the relaxation curves of the temperatures lower than the reference temperature are on the right hand side of the master curve. This can also be observed in equations A.1 and A.1. It is obvious that the logarithm of the shift factor will always be negative for temperatures higher than T_{ref} and positive for temperatures lower than T_{ref}.

APPENDIX B

HISTOGRAMS

B.1 Histgrams of average temperatures

B.1.1 January

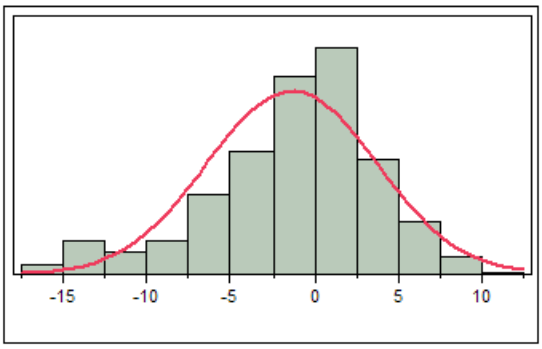

Mean	-1.332692
Std Dev	5.0305259
Std Err Mean	0.2417516
upper 95% Mean	-0.857536
lower 95% Mean	-1.807848
N	433

B.1.2 February

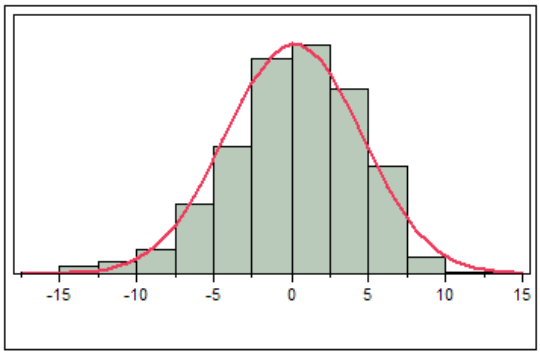

Mean	0.1589506
Std Dev	4.3629567
Std Err Mean	0.2192468
upper 95% Mean	0.5899872
lower 95% Mean	-0.272086
N	396

B.1.3 March

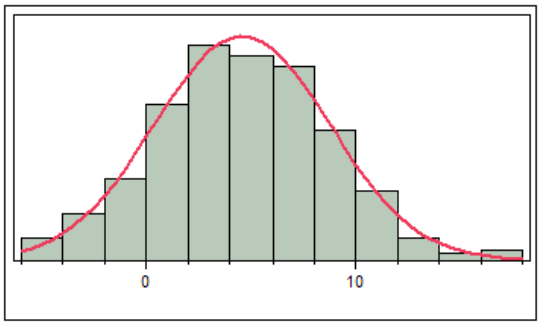

Mean	4.5695084
Std Dev	4.1882059
Std Err Mean	0.2010403
upper 95% Mean	4.9646447
lower 95% Mean	4.1743722
N	434

B.1.4 April

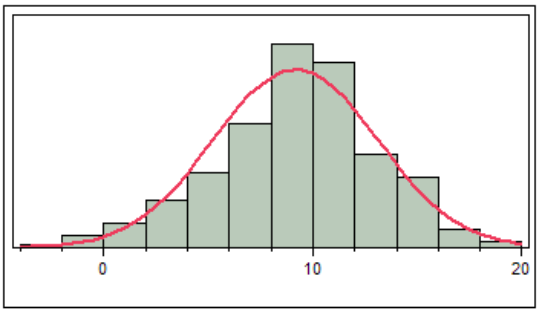

Mean	9.166251
Std Dev	3.9121063
Std Err Mean	0.1953613
upper 95% Mean	9.5503142
lower 95% Mean	8.7821879
N	401

B.1.5 May

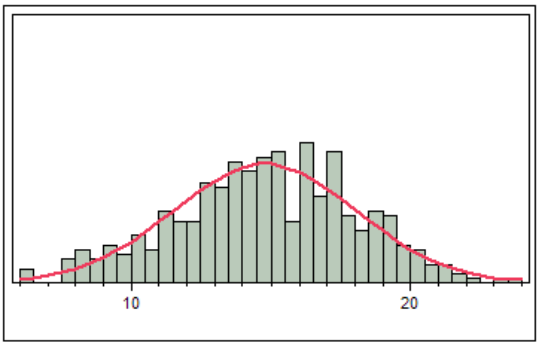

Mean	14.785911
Std Dev	3.2787244
Std Err Mean	0.1633249
upper 95% Mean	15.106989
lower 95% Mean	14.464834
N	403

B.1.6 June

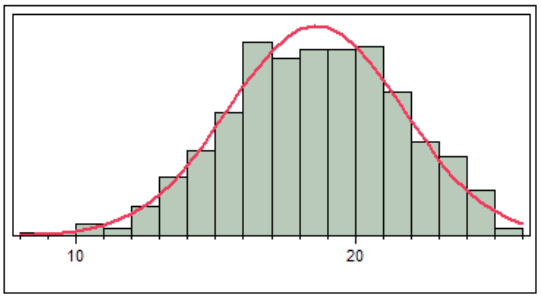

Mean	18.569516
Std Dev	3.102863
Std Err Mean	0.1579316
upper 95% Mean	18.880033
lower 95% Mean	18.259
N	386

B.1.7 July

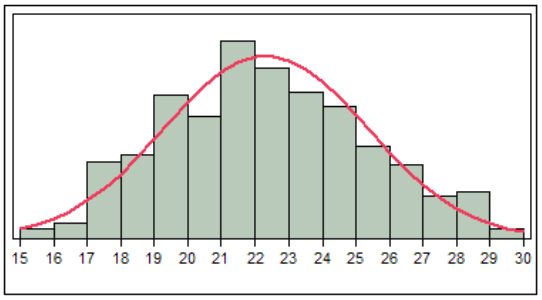

Mean	22.31941
Std Dev	3.000647
Std Err Mean	0.1494729
upper 95% Mean	22.613256
lower 95% Mean	22.025564
N	403

B.1.8 August

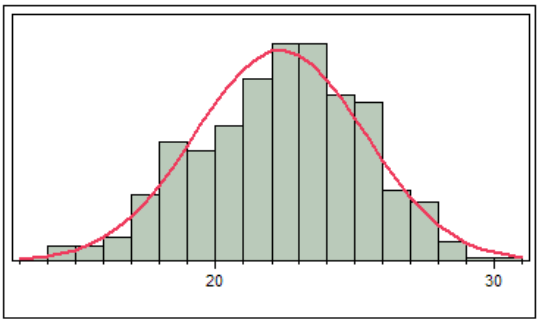

Mean	22.332919
Std Dev	3.0138645
Std Err Mean	0.1503179
upper 95% Mean	22.628428
lower 95% Mean	22.037409
N	402

B.1.9 September

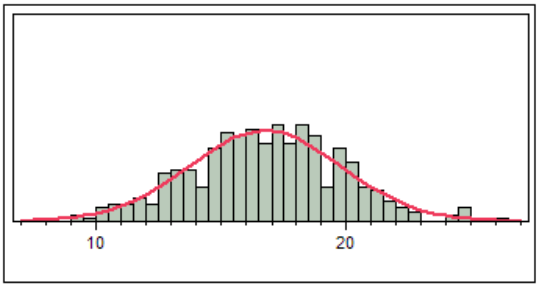

Mean	16.770655
Std Dev	3.0769944
Std Err Mean	0.1558097
upper 95% Mean	17.07699
lower 95% Mean	16.464321
N	390

B.1.10 October

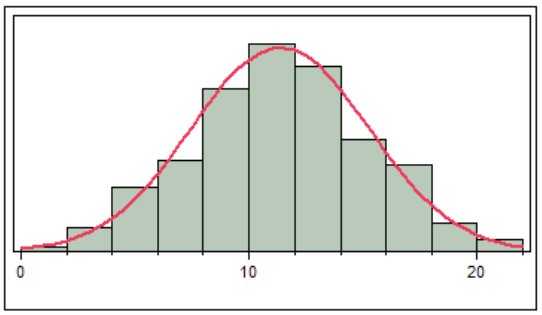

Mean	11.355252
Std Dev	3.8555232
Std Err Mean	0.1920573
upper 95% Mean	11.732814
lower 95% Mean	10.97769
N	403

B.1.11 November

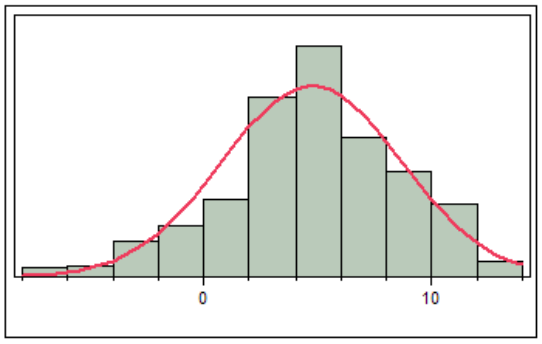

Mean	4.731339
Std Dev	3.9376322
Std Err Mean	0.1993898
upper 95% Mean	5.1233555
lower 95% Mean	4.3393226
N	390

B.1.12 December

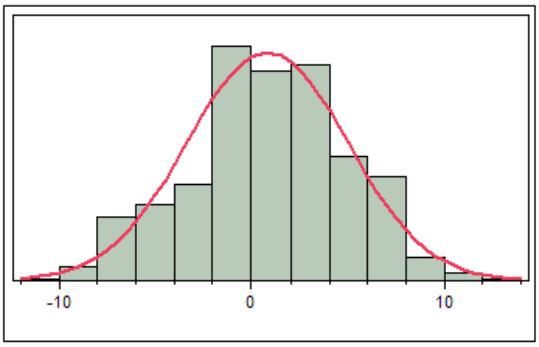

Mean	0.817878
Std Dev	4.1526958
Std Err Mean	0.2078948
upper 95% Mean	1.2265873
lower 95% Mean	0.4091688
N	399

B.2 Histograms of daily damage

B.2.1 January

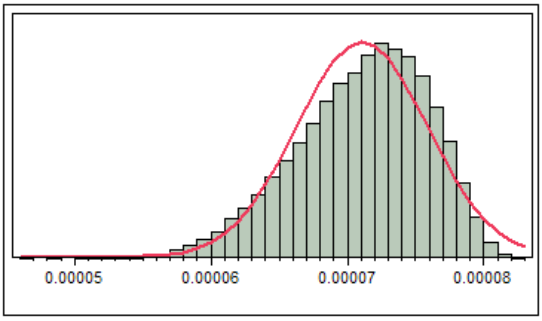

Mean	7.11E-05
Std Dev	4.80E-06
Std Err Mean	1.52E-08
upper 95% Mean	7.11E-05
lower 95% Mean	7.11E-05
N	100000

B.2.2 February

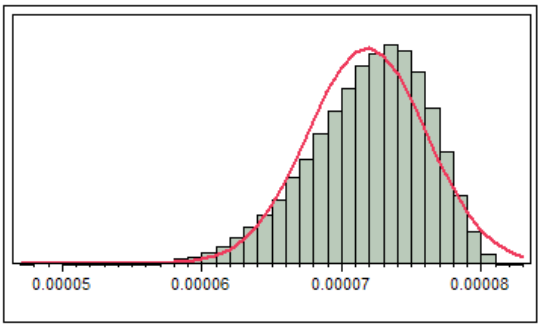

Mean	7.19E-05
Std Dev	4.23E-06
Std Err Mean	1.34E-08
upper 95% Mean	0.0000719
lower 95% Mean	7.18E-05
N	100000

B.2.3 March

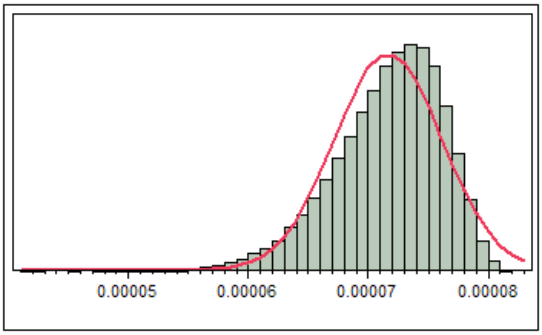

Mean	7.17E-05
Std Dev	4.48E-06
Std Err Mean	1.42E-08
upper 95% Mean	7.17E-05
lower 95% Mean	7.16E-05
N	100000

B.2.4 April

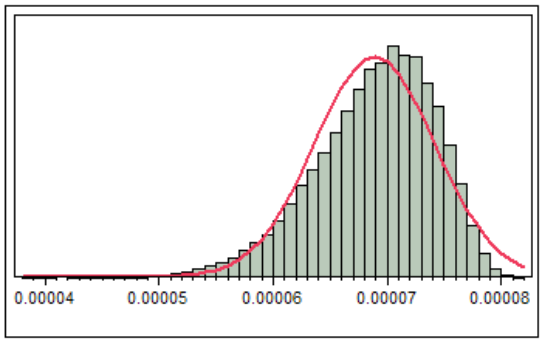

Mean	6.89E-05
Std Dev	5.26E-06
Std Err Mean	1.66E-08
upper 95% Mean	6.89E-05
lower 95% Mean	6.89E-05
N	100000

B.2.5 May

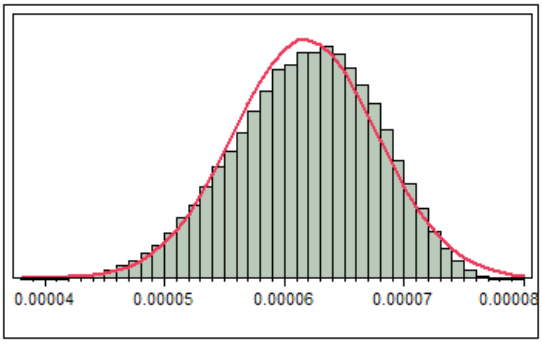

Mean	6.17E-05
Std Dev	5.98E-06
Std Err Mean	1.89E-08
upper 95% Mean	6.18E-05
lower 95% Mean	6.17E-05
N	100000

B.2.6 June

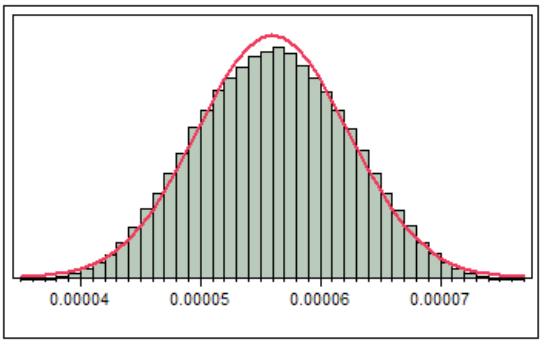

Mean	5.60E-05
Std Dev	6.28E-06
Std Err Mean	1.99E-08
upper 95% Mean	5.61E-05
lower 95% Mean	5.60E-05
N	100000

B.2.7 July

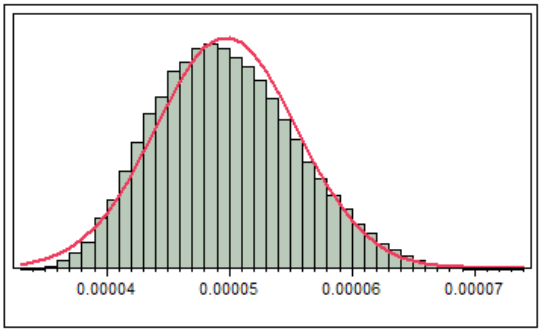

Mean	4.98E-05
Std Dev	5.75E-06
Std Err Mean	1.82E-08
upper 95% Mean	0.0000498
lower 95% Mean	4.97E-05
N	100000

B.2.8 August

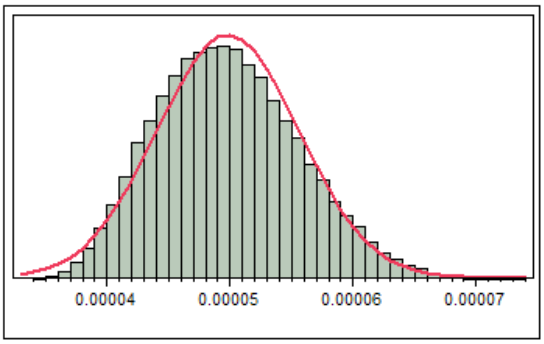

Mean	4.98E-05
Std Dev	5.77E-06
Std Err Mean	1.82E-08
upper 95% Mean	4.99E-05
lower 95% Mean	4.98E-05
N	100000

B.2.9 September

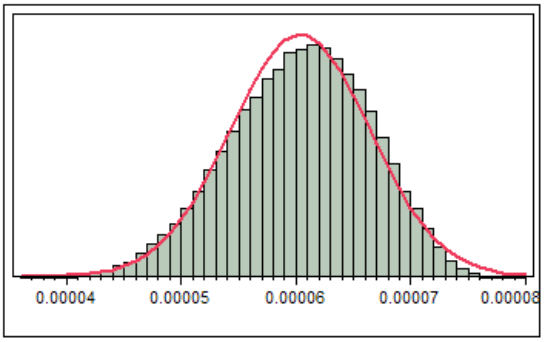

Mean	6.03E-05
Std Dev	6.09E-06
Std Err Mean	1.92E-08
upper 95% Mean	6.04E-05
lower 95% Mean	0.0000603
N	100000

B.2.10 October

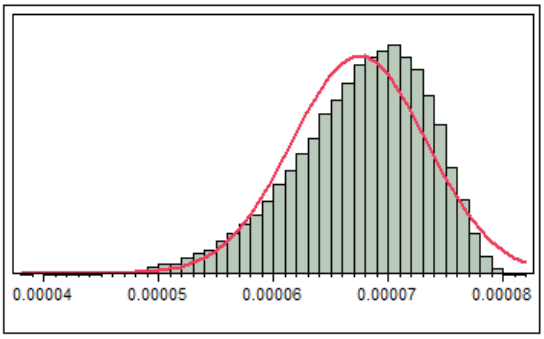

Mean	6.75E-05
Std Dev	5.86E-06
Std Err Mean	1.85E-08
upper 95% Mean	6.76E-05
lower 95% Mean	0.0000675
N	100000

B.2.11 November

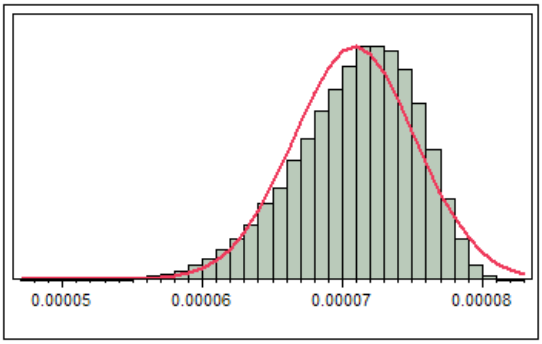

Mean	7.09E-05
Std Dev	4.36E-06
Std Err Mean	1.38E-08
upper 95% Mean	0.0000709
lower 95% Mean	7.08E-05
N	100000

B.2.12 December

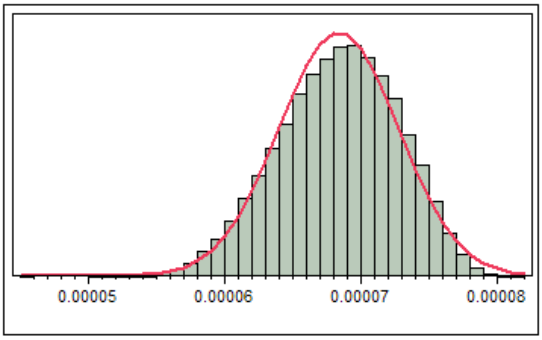

Mean	6.84E-05
Std Dev	4.37E-06
Std Err Mean	1.38E-08
upper 95% Mean	0.0000684
lower 95% Mean	6.83E-05
N	100000